JOURNAL OF GEOPHYSICAL RESEARCH, VOL. 111, B12S23, doi:10.1029/2006JB004541, 2006

Competition of magnetic and hydrodynamic forces on ellipsoidal particles under shear: Influence of the Earth's magnetic field on particle alignment in viscous media

Josef Jezek[1] and Stuart A. Gilder[2,3]

Received 1 June 2006; revised 1 September 2006; accepted 2 October 2006; published 7 December 2006.

[1] We present a model that describes the rotation of ellipsoidal magnetic particles in a viscous fluid under the influence of hydrodynamic and magnetic forces, with an aim to better understand how sediments acquire their remanent magnetizations. Analyses of the governing equations elucidate how magnetic particles will rotate for different values of leading parameters including particle shape, remanent and induced magnetic intensity, magnetic field intensity and direction, strain rate, shear direction, and viscosity. Numerical solution of the governing equations makes it possible to visualize the rotation path and the magnetic direction of a particle through time. Thus the model can discern the timescales and trajectories of magnetic particles rotating due to torque of the magnetic field couple while simultaneously entrained in a velocity gradient. For example, in a layer of viscosity 10^4 Pa s, prolate magnetite starting at any initial orientation and subjected to simple shear with a strain rate of 3.17×10^{-8} s^{-1} needs 4 months to rotate within 3° of the Earth's field direction. Under the same conditions, hydrodynamic forces will govern the orientation of oblate hematite whose moment will be perpetually randomly oriented with respect to the magnetic field direction. When applied to laboratory experiments, the viscous model successfully matches the observed data, particularly after accounting for mechanical interaction and flocculation effects. Magnetic anisotropies calculated from multiparticle systems of hematite yield typical sedimentary fabrics with relatively low percentages of anisotropy (<5%) and maximum principal axes that lie in the sedimentation plane.

Citation: Jezek, J., and S. A. Gilder (2006), Competition of magnetic and hydrodynamic forces on ellipsoidal particles under shear: Influence of the Earth's magnetic field on particle alignment in viscous media, *J. Geophys. Res.*, *111*, B12S23, doi:10.1029/2006JB004541.

1. Magnetic Recording in Sediments

[2] The typical approach to model how sedimentary rocks acquire their remanent magnetizations considers a spherical magnetic particle falling through a stagnant water column [*Rees*, 1961; *Collinson*, 1965; *King and Rees*, 1966; *Stacey*, 1972; *Hamano*, 1980; *Denham and Chave*, 1982; *Tauxe and Kent*, 1984; *Shive*, 1985; *Borradaile*, 1993; *Katari et al.*, 2000]. Viewed in this way, the particle is subject to balanced inertial, viscous and magnetic torques, and spherical magnetite particles attain perfect alignment with the ambient field virtually instantaneously (<1 s or <1 cm settling in the water column). Eventually the particles encounter the subsurface, leading to mechanical interaction. Numerical models of deposition are sensitive to the dip of the surface, grain shape anisotropy, the magnetic field direction and the statistical orientation of the grain as it rolls into niches between already deposited grains [*King*, 1955; *Griffiths et al.*, 1962]. Laboratory experiments of vertically falling particles have shown that the net effect of a depositional remanent magnetization is to shallow the remanent inclination in the rock (I_r) with respect to the applied field inclination (I_B) such that $\tan(I_r) = F \times \tan(I_B)$, where F normally ranges from 0.3 to 0.6 [*King*, 1955; *Løvlie and Torsvik*, 1984; *Tauxe and Kent*, 1984]. Misalignment of declination is negligible. From these experimental results, one would naturally conclude that all sedimentary rocks are prone to synsedimentation inclination shallowing. However, this is not always the case: sediments can yield inclinations compatible with those predicted from apparent polar wander paths and possess the same inclinations as lava flows, which are often immune to inclination shallowing [e.g., *Opdyke*, 1971] with some exception [*Urrutia-Fucugauchi et al.*, 2004]. Moreover, recent glacial and river deposits more often than not faithfully record the present or geocentric axial dipole field direction [e.g., *Granar*, 1957].

[3] More recent work has clearly shown the importance of inclination shallowing in the rock record, leading, for example, to the debate of the Baja-BC hypothesis of displaced terranes on the west coast of North America

[1]Department of Applied Mathematics and Computer Science, Faculty of Science, Charles University, Prague, Czech Republic.
[2]Institut de Physique du Globe de Paris, Equipe de Paléomagnétisme, Paris, France.
[3]Now at Ludwig Maximilians University, Department of Earth and Environmental Sciences, Geophysics Section, Munich, Germany.

0148-0227/06/2006JB004541$09.00

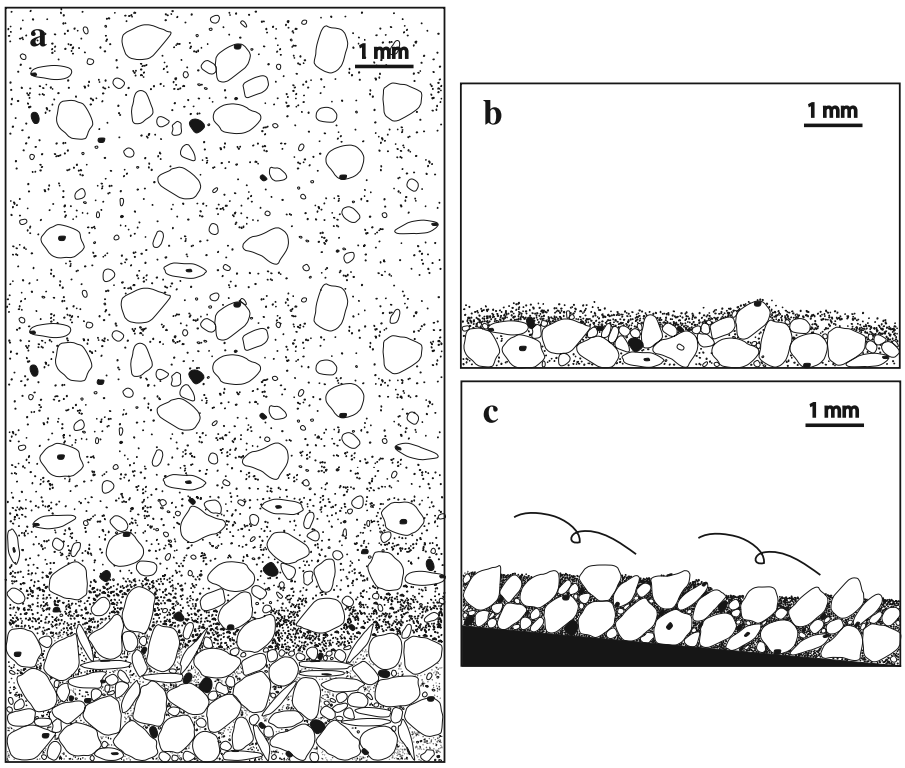

Figure 1. Possible sedimentation scenarios potentially treated by the viscous model. (a) Sedimentation in a lacustrine environment where viscosity and mechanical interaction of the particles increase with depth while particle sizes are relatively well mixed. (b) Graded-bedding scenario with differential settling based on particle size. (c) Grains deposited in a velocity gradient leading to imbrication.

[*Kodama and Ward*, 2001; *Vaughn et al.*, 2005, and references therein]. In central Asia, inclinations in Cretaceous to present continental red beds are systematically 10° to 20° shallower than coeval volcanic rocks [*Gilder et al.*, 2003]. Poleward translation estimates based on the inclination data from the red beds have led to overexaggerated amounts of intracontinental shortening associated with the India-Asia collision [*Gilder et al.*, 2001; *Tan et al.*, 2003]. On the other hand, continental red beds from eastern Asia possess steeper inclinations than those from central Asia, which means that the depositional environment and/or other factors likely play a role in the recording fidelity of such sediments. Just how environmental factors, such as stream or slope direction versus the magnetic field direction, influence the magnetic recording process in sediments is poorly known.

[4] Lending further complication to successfully understanding the lock-in process of magnetization in sediments is that particle alignment often changes after initial deposition. For example, *Irving and Major* [1964] showed that magnetite or hematite-rich sediments first deposited in a null field, then subjected to an applied field, accurately recorded the field direction. Thus postdepositional effects such as dewatering, earthquakes, tangential stress from fluid flow, etc., could play a significant role in influencing the final orientation of the magnetic vector [e.g., *Kent*, 1973; *Tucker*, 1980]. However, several laboratory experiments are inconsistent with postdepositional reorientation of magnetic particles [e.g., *Verosub et al.*, 1979; *Katari et al.*, 2000]. Numerical modeling by *Shcherbakov and Shcherbakov* [1987] suggests that postdepositional processes only account for ~10% of a sediment's total magnetization.

[5] Laboratory redeposition experiments in running water (e.g., that include a shear component) on inclined beds can produce significant deviations depending on current direction, magnetic field direction, bedding slope, particle size, etc. [*King*, 1955; *Rees*, 1961, 1964, 1971; *Griffiths et al.*, 1962; *Hamilton and King*, 1964; *Hamilton et al.*, 1968; *Rees and Woodall*, 1975]. Numerical models of this more complicated scenario have been limited to two-dimensional spherical particles rolling on the surface. Other work has considered particle alignment after lithification (e.g., after the remanence has been locked in), such as due to compaction or tectonic strain [*Rees*, 1979; *Kodama and Goldstein*, 1991; *Kodama and Sun*, 1992; *Borradaile*, 1993; *Jackson et al.*, 1993, and references therein]. Indeed, even for these latter cases concerning relatively solid material, *Kodama* [1988] and *Borradaile* [1993] found that the influence of strain on magnetic recording could be treated with a rigid marker approach, which is equivalent to a viscous model.

[6] The sedimentation process spans a vast amount of possibilities regarding particle size and shape distributions, viscosity, pH and Eh of the fluid, flow/shear of the newly sedimented layer, etc. Moreover, diagenetic effects, contact forces between particles and Brownian motion should be considered [see *Tarling and Turner*, 1999, and references therein]. To our knowledge, no existing model covers all these effects. Also, the same goes for our model: it can be regarded as a simplified end-member case. Figure 1 shows a few environments where we think the viscous model is

applicable. They are relevant to fluvio-lacustrine (continental) depositional regimes, such as in a shallow lake near the foreland of a mountain belt. Figure 1a depicts a progression in sedimentation near the middle of a lake, where viscosity and mechanical interaction of the particles increase with depth while particle sizes are relatively well mixed. The ideal case occurs at the beginning stages when noninteracting particles fall through the water column. Potential electrostatic attraction between clay particles and magnetic grains (flocculation) might cause the two to adhere, in which case the assemblage would still respond to torque of the magnetic field, yet the volumetric magnetic moment is reduced and the particle shape is different [*Katari and Bloxham*, 2001]. For example, *Anson and Kodama* [1987] pointed out that magnetic particles attached to clay particles electrostaticly. *Deamer and Kodama* [1990] tested this phenomena experimentally and *Sun and Kodama* [1992] provided experimental evidence and a model showing that magnetic particles attach to clay particles by either electrostatic forces or van der Waals forces, which then become incorporated into the clay fabric of the sedimentary rock and rotate with the clay particles during postdepositional processes. Toward the bottom, mechanical interaction would arrest movement of the large particles while a magnetic torque could still realign smaller grains in the interstices. Another scenario represents graded bedding where the largest grains settle out first (Figure 1b), in which case one would have to account for different settling times of the particles.

[7] Where slopes and currents exist near lake margins (Figure 1c), the velocity profile at the bottom is steep and the particles may be slightly imbricated. The slurry at the bottom, to some finite depth, could be considered as a viscous fluid that can flow under gravity and water currents. One example is to consider a steady, unidirectional flow of a viscous fluid down an inclined plane. Following *Turcotte and Schubert* [1982, p. 235], the top of a few centimeters thick muddy slurry deposited on a 1° slope can flow several centimeters to a few meters over yearly timescales depending on the viscosity. Magnetic particles entrained in such slurries are then reoriented by competing hydrodynamic and magnetic forces.

[8] Below we present a model that describes the rotation of an ellipsoidal magnetic particle immersed in a viscous fluid under the simultaneous influence of hydrodynamic and magnetic forces. The model provides insight into the possible types of motion that a particle might undergo during sedimentation or within a slowly flowing or creeping soft sediment (mud). The iron oxides of magnetite and hematite contribute most often to the magnetic remanence in sedimentary rocks, so they are treated here. The ability of these minerals to be aligned by an external magnetic field from both remanent and induced magnetic force couples is considered. The model is new in that it applies a viscous approach to ellipsoidal particles (instead of spheres) that are magnetic and rotate in response to an induced field and that it also involves flow (shear) of the fluid in which the particles are immersed. Multiparticle systems can also be treated to study affects of preferred orientation so that we can simultaneously model the development of both remanent magnetization and magnetic fabric. In this article, we develop the theory and show the basic properties of the model, especially time constants of the alignment process in different hypothetical conditions. We then apply the model to experimental data.

2. Rotation of a Rigid Particle in Viscous Flow

[9] *Jeffery* [1922] described the rotation of a rigid, ellipsoidal particle in a viscous flow. The equations of particle rotation can be written as

$$\omega_1 = B_1 E_{32} - \Omega_{32}, \quad \omega_2 = B_2 E_{13} - \Omega_{13}, \quad \omega_3 = B_3 E_{21} - \Omega_{21}, \tag{1}$$

where ω_i, $i = 1, 2, 3$, are the angular velocities of the particle around its axes, $\mathbf{E}$ and $\mathbf{\Omega}$ denote the symmetric and asymmetric part of the velocity gradient tensor, and the shape parameters

$$B_1 = \frac{b^2 - c^2}{b^2 + c^2}, \qquad B_2 = \frac{c^2 - a^2}{c^2 + a^2}, \qquad B_3 = \frac{a^2 - b^2}{a^2 + b^2} \tag{2}$$

characterize the ellipsoidal particle with semiaxis dimensions a, b and c, where $a > b > c$. Given the flow (velocity gradient tensor), the particle axial ratio, and its starting position, the particle trajectory during flow can be solved by equations (1), which are written in the coordinate system rotating with the particle. In this system, the velocity gradient tensor is a function of the instantaneous orientation of the particle with respect to a coordinate system fixed in space, and thus causes problems in integration. Only some analytical solutions of the equations have been found for rotating ellipsoids in specific flow types such as simple shear [*Jeffery*, 1922], pure shear [*Gay*, 1968], axial flattening [*Debat et al.*, 1975; *Tullis*, 1976], general orthorhombic [*Fernandez*, 1988], and coaxial flow mixed with simple shear [*Jezek et al.*, 1996]. Other work has discussed the applicability of the Jeffery's model to geological problems [e.g., *Kodama*, 1988; *Ildefonse et al.*, 1997; *Arbaret et al.*, 2000]. Software was published for modeling particle rotation [*Jezek*, 1994] and for modeling flow around a rotating particle using the Jeffery approach [*Jezek et al.*, 1999]. *Willis* [1977] found that the equations of type (1) also hold for broader classes of prismatic bodies.

3. Coupling of Hydrodynamic and Magnetic Forces

[10] Consider that an ellipsoidal magnetic particle rotates in a viscous fluid in the presence of an external magnetic field ($\mathbf{B}$). The magnetic orienting couple (C^M) acting on the magnetic particle of remanent magnetization per unit volume ($\mathbf{J_v}$) and magnetic susceptibility ($\mathbf{K}$) in a magnetic field of intensity ($\mathbf{H}$) is

$$\mathbf{C}^M = V(\mathbf{J}_V + \mathbf{KH}) \times \mathbf{B}, \tag{3}$$

where V is the particle volume and $\mathbf{K}$ is treated as the volumetric susceptibility tensor placed in the particle coordinate system as

$$\mathbf{K} = \begin{pmatrix} K_1 & 0 & 0 \\ 0 & K_2 & 0 \\ 0 & 0 & K_3 \end{pmatrix} \tag{4}$$

with K_1, K_2, and K_3 being the principal susceptibilities. K_1 is in the long axis direction of prolate particles or in the basal plane of oblate particles.

[11] Now we compare both the magnetic and hydrodynamic couples acting on the particle using the equations for the hydrodynamic couple developed by *Jeffery* [1922]. In the particle coordinate system that rotates with the particle, the components of the hydrodynamic couple are (*Jeffery*'s [1922] equations (36) written in our notation):

$$\begin{aligned} C_1^H &= \frac{16\pi\mu}{3(b^2\beta_0 + c^2\gamma_0)}\left\{\left(b^2 + c^2\right)E_{32} - \left(b^2 + c^2\right)(\Omega_{32} + \omega_1)\right\}, \\ C_2^H &= \frac{16\pi\mu(c^2 + a^2)}{3(c^2\gamma_0 + a^2\alpha_0)}\left\{\left(c^2 + a^2\right)E_{13} - \left(c^2 + a^2\right)(\Omega_{13} + \omega_2)\right\}, \\ C_3^H &= \frac{16\pi\mu(a^2 + b^2)}{3(a^2\alpha_0 + b^2\beta_0)}\left\{\left(a^2 + b^2\right)E_{21} - \left(a^2 + b^2\right)(\Omega_{21} + \omega_3)\right\}, \end{aligned} \tag{5}$$

where ω_i, $i = 1, 2, 3$, are the angular velocities of the particle around its axes. The geometric parameter (α_0) is

$$\alpha_0 = \int_0^\infty \frac{d\lambda}{(a^2 + \lambda)\sqrt{(a^2 + \lambda)(b^2 + \lambda)(c^2 + \lambda)}}, \tag{6}$$

with similar expressions holding for β_0 and γ_0 (λ is the variable of integration). These parameters can be computed numerically [*Jezek et al.*, 1999] or, in cases where ellipsoids have two equal axes, an analytical expression can be found (see Appendix A). Note that when the ellipsoid becomes a sphere ($a = b = c = r$), the equations for the force couple reduce to the well known formulae for the hydrodynamic couple acting on a sphere $8\pi\mu r^3\omega$ [*Happel and Brenner*, 1983, p. 227].

[12] Now adding the magnetic and hydrodynamic force couples (equations (3) and (5)), and assuming that the resultant couple is zero (following *Jeffery* [1922] and *Nagata* [1961], inertial forces are neglected), we obtain, after rearranging, the equations for angular velocities:

$$\begin{aligned} \omega_1 &= \frac{b^2 - c^2}{b^2 + c^2}\,E_{32} - \Omega_{32} + \frac{3(b^2\beta_0 + c^2\gamma_0)}{16\pi\mu(b^2 + c^2)}C_1^M \\ \omega_2 &= \frac{c^2 - a^2}{c^2 + a^2}\,E_{13} - \Omega_{13} + \frac{3(c^2\gamma_0 + a^2\alpha_0)}{16\pi\mu(c^2 + a^2)}C_2^M \\ \omega_3 &= \frac{a^2 - b^2}{a^2 + b^2}\,E_{21} - \Omega_{21} + \frac{3(a^2\alpha_0 + b^2\beta_0)}{16\pi\mu(a^2 + b^2)}C_3^M \end{aligned} \tag{7}$$

The equations of particle rotation are again written in the particle coordinate system, where the hydrodynamic and magnetic parameters are recomputed for every particle orientation, yet the particle parameters of shape, remanent magnetization, and susceptibility remain constant. Only in some very particular cases do the equations have analytical solutions; however, they can be solved numerically by techniques similar to those of *Jezek* [1994]. Describing the rotation of the particle with respect to the fixed coordinate system by means of the Euler angles ϕ, θ and ψ and by using the known relations between the angular velocity and the time derivatives of the Euler angles, we obtain three differential equations:

$$\begin{aligned} &\phi = (\omega_1 \sin\psi + \omega_2 \cos\psi)/\sin\theta, \quad \theta = \omega_1 \cos\psi - \omega_2 \sin, \\ &\psi = \omega_3 - \phi\cos\theta. \end{aligned} \tag{8}$$

These equations can be solved numerically as an initial value problem. Given the velocity gradient tensor, the axial ratio of the particle, its magnetic parameters, the magnetic field vector, and initial values of the Euler angles (the initial orientation of the particle), we can compute the time evolution of the Euler angles, e.g., the particle's rotation. This procedure will be used for examples given in the following text. The final terms on the right-hand side of equations (7) represent the deviation from pure hydrodynamic rotation. When no hydrodynamic shear acts on the particle (when the velocity gradient is zero), the first and second terms on the right hand side of equations (7) disappear, and the equations describe the magnetic alignment of ellipsoidal particles in a static viscous fluid.

4. Analysis of a Simple but Important Case

[13] To gain insight into the character of equations (7), we discuss a simple case of a magnetic particle rotating in the vertical plane containing the magnetic field vector. In this scenario, the influence of both magnetic and hydrodynamic forces on the grain's magnetic declination is zero, which restricts the grain's magnetic vector to rotate within a single plane (2D case). This allows us to simplify the governing equations to explore how the magnetic inclination of a particle will be affected depending on the proportion of magnetic to hydrodynamic field parameters as a function of flow direction. Let the magnetic field (**B**) have declination (D_B) and inclination (I_B); the x-y plane of our coordinate system is horizontal, with +x oriented to the north and +z oriented downward. Horizontal simple shear (where γ represents shear rate) is oriented toward the north (i.e., the rotational axis of simple shear is parallel to the $-y$ axis direction) as sketched in Figure 2. Shear is dextral in this case and sinistral when the rotational axis is in the $+y$ axis direction. The magnetic particle is a prolate ellipsoid whose remanent magnetization (J_V) is oriented along its long (a) axis (axial ratio 2:1:1) which lies in the x-z plane. The angle between the magnetic field direction (I_B) and the a axis of the particle is denoted as δ. Positive δ values indicate that the magnetic inclination of the particle (I_r) is greater than I_B.

[14] From equation (7), it follows that the particle rotates in the x-z plane, e.g., in the plane defined by the flow and field directions, with an angular velocity of

$$\omega = \dot{\delta} = 0.3\gamma\left(-\cos 2(I_B + \delta) + 1.6667 - 0.3697\frac{J_V B}{\mu\gamma}\sin\delta\right) \tag{9a}$$

for dextral simple shear and

$$\omega = \dot{\delta} = 0.3\gamma\left(\cos 2(I_B + \delta) - 1.6667 - 0.3697\frac{J_V B}{\mu\gamma}\sin\delta\right) \tag{9b}$$

for sinistral simple shear (see Appendix B for derivation). From equations (9a) and (9b), the character and especially the sign of ω, i.e., the sense of rotation, depends on I_B and the ratio of the magnetic and hydrodynamic force couple:

$$Qmh = \frac{J_V B}{\mu\gamma}. \tag{10}$$

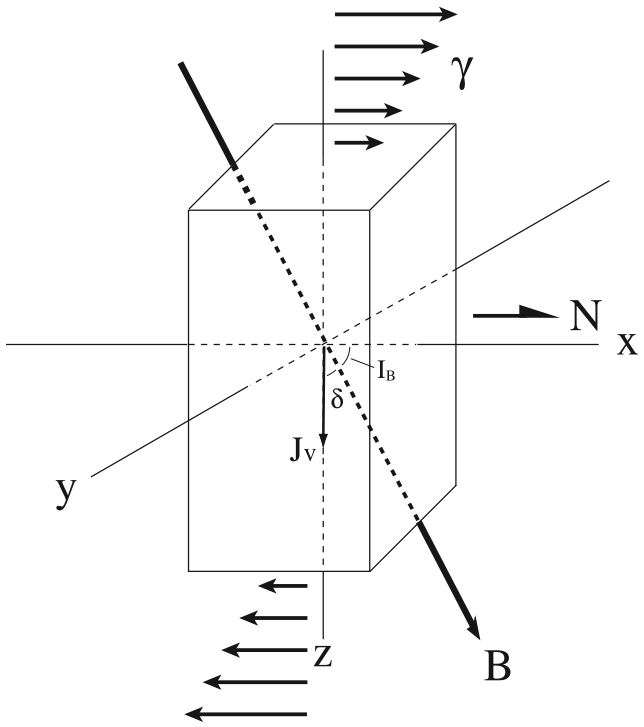

Figure 2. Diagram showing the orientation of a magnetic particle, with magnetic vector J_V in space. The *x*-*y* plane is horizontal with +*z* positive downward. True north is in the +*x* axis direction. Arrows in the *x*-*z* plane indicate the simple shear (γ) velocity field. Other symbols are **B**, magnetic field vector; I_B, magnetic field inclination; δ, angle between I_B and the magnetic inclination of the particle.

For the moment, we neglect induced magnetization. γ is the strain rate and μ is viscosity, as above.

[15] Possible types of magnetic particle behavior are shown in Figure 3, where I_B is chosen to be 50°, e.g., the field inclination points down to the north. Figure 3 (top) (bottom) corresponds to dextral (sinistral) simple shear with the shear direction acting toward (or away from) the magnetic field direction. When *Qmh* is $\gg$100, the particle will orient parallel to the magnetic field direction starting from any initial orientation (Figures 3a and 3f), except when initially oriented exactly antipodal (180°) to the field direction. Thus two angles (δ) at zero angular velocity are possible. One (δ_L) represents an orientation of labile (unstable) equilibrium, which is attained only by particles having this initial orientation with respect to the field direction. These particles do not rotate but, from a statistical viewpoint, they are negligible. For all other starting positions, particles rotate toward a stable final orientation of δ_S with respect to I_B. As *Qmh* decreases (by decreasing [increasing] magnetic [hydrodynamic] forces), these two angles change. The situation is shown for *Qmh* ≈100 in Figures 3b and 3g for dextral and sinistral shear, respectively. The value $|\delta_S|$ increases with decreasing *Qmh*, and δ_S approaches δ_L (compare Figures 3b and 3g where *Qmh* ≈ 100 with Figures 3c and 3h where *Qmh* ≈ 5). If *Qmh* decreases even further, at a certain value of *Qmh* (2.25 for the dextral case), δ_S and δ_L become equal, and a particle will rotate in the sense of simple shear until stopping at an angle, δ_0, from the magnetic field direction when its angular velocity is zero (Figure 3d). A similar effect occurs for the sinistral case (Figure 3i). Below *Qmh* = 2.25, no stable orientation with respect to the magnetic field direction is reached, and the particle rotates indefinitely in the sense of simple shear (Figures 3e and 3j). Note that the angular velocity of the particle is not constant. For *Qmh* near 2.25, the minimum angular velocity occurs near δ_0 (see Figures 3d and 3i). For lower *Qmh* values, the angular velocity minimum occurs when the particle's long axis crosses the simple shear plane (x-y plane in Figure 2).

[16] In sum, we see that between cases dominated by either magnetic (*Qmh* $\gg$ 100) or hydrodynamic (*Qmh* < 2.25) forces, a transition interval of *Qmh* values exist over which the final orientation of a magnetic particle deviates significantly from the applied field direction. For dextral simple shear, it can be shown by a Taylor series approximation that for *Qmh* > 10, the deviation (δ_S) from I_B can be well approximated as

$$\delta s = (\cos 2I_B - 1.6667)/(2\sin 2I_B - 0.3697Qmh), \qquad (11)$$

which is plotted against *Qmh* in Figure 4 for a variety of inclination values (curves with positive δ_S). The corresponding deviation is not exactly the same for sinistral shear, but in absolute value, it is not too different from the previous case (curves with negative δ_s in Figure 4). For any north directed field inclination and *Qmh* less than 100, δ_s will be greater in steep magnetic fields than in shallow magnetic fields, e.g., δ_s increases with increasing I_B (Figure 4, insets). When *Qmh* is greater than about 50, δ_s is within ±10° of I_B for both cases. This indicates that the magnetic inclinations of particles entrained in suspensions (mud) that flow to the north in a north directed field would be systematically steeper than the field, while the magnetic inclinations of particles entrained in suspensions (mud) that flow to the south in a north directed field would be systematically shallower than the field.

5. General Case

[17] For the general case, we cannot make a simple presentation of the governing equations (7) as above, but we can discuss the relative importance of individual terms in equations (7), or we can compare the magnetic and hydrodynamic force couples. When also considering the effects of induced magnetization, the relative magnitude of hydrodynamic, permanent magnetic and induced magnetic force couples are given by the products of parameters μ, γ, B, J_V, ΔK:

$$q\mu\gamma, \qquad J_V B, \qquad \Delta K B^2/\mu_0, \qquad (12)$$

where ΔK is the difference between the maximum and minimum principal susceptibility, μ_o is the permeability in a vacuum, and q is the particle shape factor, which is between about 5 and 12 (e.g., for a prolate particle of axial ratio 2:1:1, q = 7.2; for an oblate particle 4:4:1, q = 10.2).

[18] The relationship among force couples in equations (12) is plotted in Figure 5 for three representative magnetic particles: magnetite with shape axial ratio = 2:1:1, J_V =

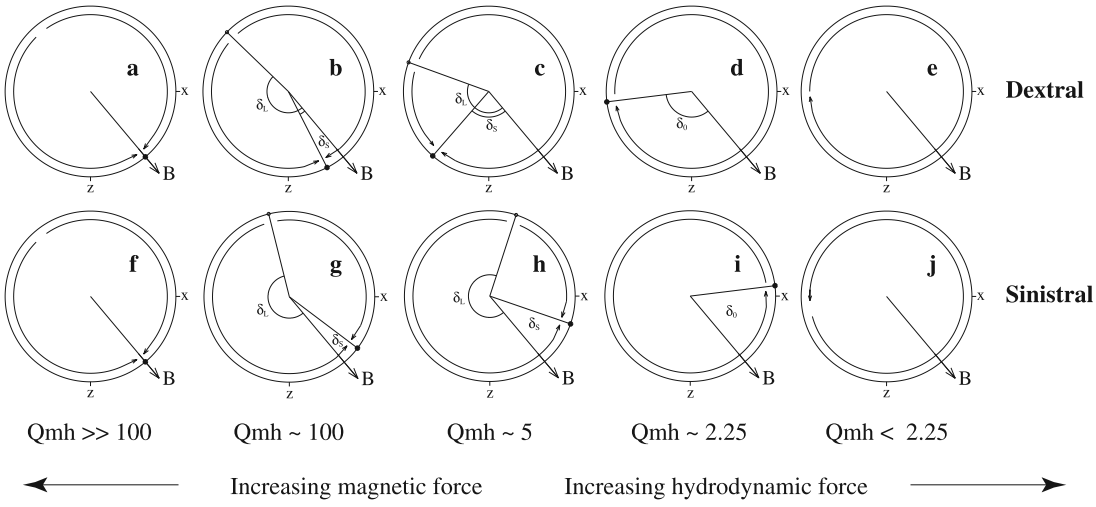

Figure 3. Possible rotation paths of the inclination of magnetic particles depending on the ratio of the magnetic and hydrodynamic force couples (*Qmh*). Figures 3a–3j show sections in the x-z plane, with +x oriented to the north and +z oriented downward. **B** is the magnetic field vector lying within the x-z plane and the lines with small solid black circles indicate the magnetic vector direction of a prolate grain. In magnetically dominated cases ($Qmh \gg 100$), magnetic particles reorient parallel to the magnetic field; whereas in hydrodynamically dominated cases ($Qmh < 2.25$), particles rotate cyclically due to simple shear and will never attain a stable (constant) inclination. For intermediate cases, at zero angular velocity, the magnetic inclination of the particle lies at angles δ_S and δ_L away from I_B. The parameter δ_L represents an orientation of labile (unstable) equilibrium, which is attained only by those particles having that particular initial orientation with respect to the field direction. They are statistically negligible. For all other starting positions, particles rotate toward a stable final orientation of δ_S with respect to I_B. The value $|\delta_S|$ increases with decreasing *Qmh*, and δ_S approaches δ_L (compare Figures 3b and 3g where $Qmh \approx 100$ with Figures 3c and 3h where $Qmh \approx 5$). At a certain value of *Qmh* (2.25 for the dextral case), δ_S and δ_L are equal and a particle will rotate in the sense of simple shear until stopping at δ_0 (Figure 3d).

1000 A m^{-1}, and $\Delta K = 0.002$ (SI) and two hematite particles with shape axial ratios of 4:4:1, with $J_V = 4$ A m^{-1} and $\Delta K = 0.022$ and 0.23 (SI). The susceptibility value for magnetite is from *Collinson* [1983] and those for hematite are from *Collinson* [1983] and *Hrouda* [2002], respectively. For the J_V of magnetite, we follow *Rees and Woodall* [1975], who considered a value of 1000 A m^{-1} to be fairly typical of magnetite-bearing, fine-grained sediments. This value is within the range of that considered by *Katari and Bloxham* [2001] (between 10^2 and 10^4 A m^{-1}), following *Stacey* [1972]. As the J_V of hematite is 250 times less than magnetite [*Collinson*, 1983], we take 4 A m^{-1} as a typical value for hematite-bearing, fine-grained sediments. In Figure 5, $B = 5 \times 10^{-5}$ T and the viscosities considered here range from above water (10^{-3} Pa s) to about 10^6 Pa s in mud [*Migniot*, 1989a, 1989b]. We plot the curves where the relative hydrodynamic force couples are equal to those of remanent and induced magnetization for magnetite and hematite in $\gamma - \mu$ coordinates. On a logarithmic scale, the curves become lines, with each line dividing the $\gamma - \mu$ plane into domains dominated by hydrodynamic forces above the line from those dominated by magnetic forces below the line. Note that in the second case of hematite, which uses the extremely high crystalline anisotropy susceptibilities following *Hrouda* [2002], the permanent and induced couple lines are almost identical.

[19] From the definition of simple shear, for two points placed vertically one above other at a distance Δz, the upper point has velocity $v = \gamma \Delta z$, relative to the lower point. So, a strain rate of $\gamma = 3.17 \times 10^{-8}$ s^{-1} implies that the upper point lying in a 10-cm-thick layer moves 10 cm in 1 year (angular shear strain = 1). From the governing equations, we can investigate how much time it takes for a particle to

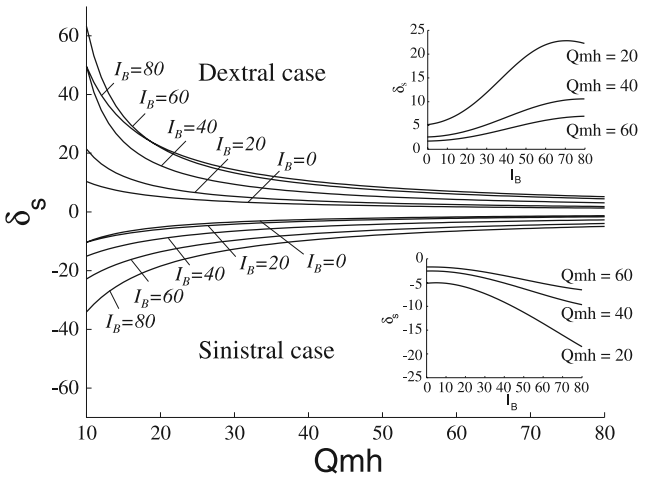

Figure 4. Angular deviation (δ_s) of the particle inclination (I_r) from the applied field inclination (I_B) for cases where both magnetic and hydrodynamic forces influence particle motion (*Qmh* between 10 and 80). Insets show δ_s values versus of I_B under constant *Qmh* conditions. Positive (negative) values of δ_s signify that the particle inclinations are greater (less) than the field inclination.

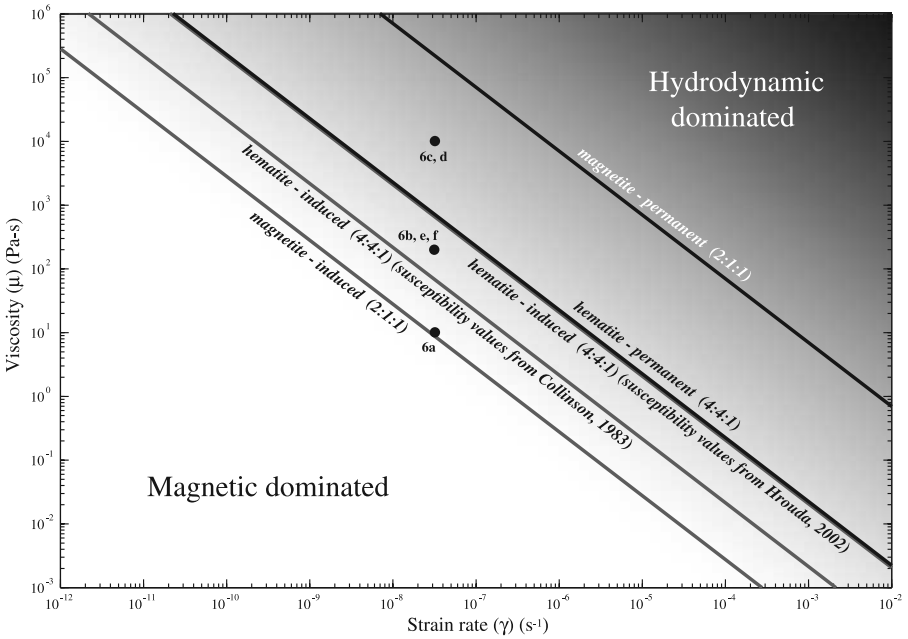

Figure 5. Relationship among magnetic and hydrodynamic force couples acting on magnetite and hematite particles, plotted in strain rate (γ) versus viscosity (μ) space. The area above the $\gamma - \mu$ line for each example is dominated by hydrodynamic forces, while magnetic forces prevail below the line. Black lines correspond to remanent magnetizations while gray lines correspond to induced magnetizations. Solid circles with letters represent the $\gamma - \mu$ conditions of the examples shown in Figure 6.

orient parallel to an external field, or observe the angular difference between the particle and field directions at a given time when subject to varying hydrodynamic and magnetic conditions. We have done so in Figure 6 by numerical solution of equation (7), which shows example cases when oblate hematite and prolate magnetite particles are sheared in fluids of viscosities and shear rates specified in Figures 5 and 6 in a magnetic field oriented $D_B = 0°$ and $I_B = 50°$, similar to the present field in central Asia. Simple shear planes are parallel to the x-y plane, i.e., the plane of Figures 5 and 6, and arrows indicate their sense in the upper half-space ($z > 0$). Each example contains three particles starting at different orientations and the trajectories of the magnetic vectors are indicated. Figures 6a and 6b show that hematite takes 2 months to orient itself parallel to the magnetic field in a 10 Pa s fluid whereas magnetite takes only two days in a fluid whose viscosity is 20 times greater. Figures 6c and 6d are similar examples except that the viscosities are 10^4 Pa s in both cases. One sees that magnetite becomes aligned with the field after 4 months whereas hematite is dominated by hydrodynamic forces and will never attain a stable orientation with respect to the field direction. Figures 6e and 6f show the effect of shear direction on the final orientation of a hematite particle rotating in a fluid of the same viscosity (200 Pa s). After 2 years, the three particles rotating under conditions with shear acting in the field direction reach an equilibrium position where I_r is about 10° greater than I_B (Figure 6e), whereas when shear acts in the opposite direction, I_r is about 10° less than I_B (Figure 6f). This is in agreement with values shown in Figure 4 for $Qmh = 33$, where δ_s is within ±10°.

[20] Finally, Figures 6g and 6h treat hematite using the susceptibilities from *Hrouda* [2002] where the remanent and induced couples are of the same order. No simple shear acts on the particles (*Qmh* is thus undefined as the strain rate is null), but viscous forces are still present to oppose magnetic reorientation. Figure 6g is similar to the preceding cases where the trajectory of the remanence vector is shown; whereas in Figure 6h, the trajectory tracks the poles of the basal planes of hematite particles A, B, and C from Figure 6g. Although the remanence vector eventually reaches parallelism with the external field, the path in doing so is complicated by the fact that the basal planes first align with the external field (e.g., the poles to the basal planes go to the plane perpendicular to the field as in Figure 6h). Once this is accomplished, the grains rotate about these poles until the remanence vector catches the field (Figure 6g).

6. Application of a Viscous Model to Particle Alignment During Sedimentation

[21] In order to demonstrate the applicability of the model to real world experimental data, we turned to the literature. However, it is difficult to find results that unambiguously document time variations in magnetic declination, inclination, and intensity during sedimentation, especially in sediments whose magnetic grain size distributions are well known. To the best of our knowledge, only the *Tauxe and Kent* [1984] (hereinafter referred to as TK84) experiments were described in enough detail to appropriately apply our viscous model. Their experiments, briefly repeated here, used sediments collected from the Soan River, Pakistan. Approximately 10 g of dry sediment were weighed and mixed with water, then put into plastic tubes 3.5 cm in

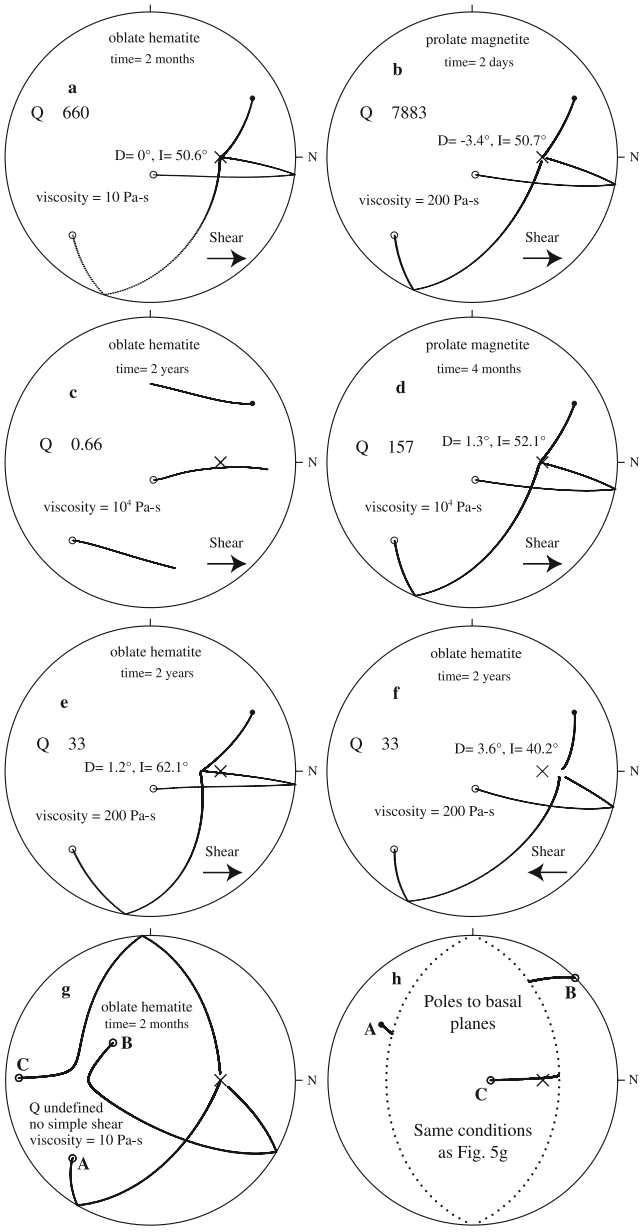

Figure 6. Time evolution of the rotation of hematite and magnetite grains computed by numerical solution of equation (7). Parameters of individual cases are described in the text and indicated in Figure 5. The declination (D) and inclination (I) written in the stereonet corresponds to the particle starting from the left lower quadrant of the stereonet. The cross is the magnetic field direction ($D_B = 0°$, $I_B = 50°$ in each figure). Solid and open circles (lower and upper hemisphere, respectively) represent the starting position of the long axis for prolate grains (parallel to the magnetic vector in the grain) or the magnetic vector direction in the basal plane for oblate grains (hematite). Trajectories correspond to J_v in Figures 6a to 6g and the poles to the basal planes of the hematite particles in Figure 6h. Particles A, B, and C are the same in Figures 6g and 6h. Susceptibility values are from *Collinson* [1983] in Figures 6a to 6f and from *Hrouda* [2002] in Figures 6g and 6h.

diameter and 15 cm in height. The tubes were sealed, agitated and then placed in a controlled field for about 5 hours. Several experiments were performed. In one set, they found that the remanent intensity of the redeposited sediment varied as a function of the applied field intensity (H) and field inclination (I_B). In another, they determined that the amount of inclination shallowing, e.g., the ratio of the inclination recorded in the rock (I_r) to I_B, is independent of H. Finally, they confirmed that the relationship between I_r and I_B followed the equation $\tan(I_r) = F \times \tan(I_B)$, with F being equal to 0.55 for the Soan River sediments. *Tauxe and Kent* [1984] then explored whether a viscous model could explain their experimental results. They found that particles would align too fast compared to their fall durations, which led them to reject the viscous model as a feasible explanation. Here, we reexamine the *Tauxe and Kent* [1984] study. We show that we can reproduce their results and conclude that a viscous model is indeed a viable possibility to explain the data.

6.1. Parameters

[22] The key parameters needed to model the TK84 data are the size distribution of the magnetic particles and knowledge of how the remanence of the sedimented fraction increases with time. TK84 (p. 557) state that the sediment was composed of a clay fraction (diameter D < 4 μm) comprising 21% (by weight) and of a silt plus sand fraction (D > 4 μm) comprising 79%. Both fractions contain hematite. After settling in a 55 μT field with an inclination of 70°, the clay fraction acquired a remanent intensity of 7.0×10^{-5} A m^2 kg^{-1}, while the silt plus sand was 1.8×10^{-5} A m^2 kg^{-1}. The total remanence of the sediment (J_T) was then $0.21*(7 \times 10^{-5}) + 0.79*(1.8 \times 10^{-5}) = 2.892 \times 10^{-5}$ A m^2 kg^{-1}, with each size fraction contributing roughly equal proportions to J_T.

[23] From these observations, one can establish a list of conditions that must be accounted for by the model. The first condition (C1) is that about $0.5J_T$ is created by magnetic particles with D < 4 μm and $0.5J_T$ with D > 4 μm. Further information provided in TK84 is that after five minutes of settling, the sediment (both clay and silt plus sand components) had acquired 1/3 of J_T (condition C2) and after one hour, 1/2 of J_T was acquired (condition C3). We assume that only the sedimented fraction, i.e., approximately the bottom ~0.5 cm of the tube, contributes to J_T. On the basis of conditions C1, C2 and C3 it is possible to construct a hypothetical composition of the sediment. Following TK84, we consider platy hematite of D (diameter) and T (thickness) with the ratio T = D/10.

6.2. Alignment in a Magnetic Field

[24] One needs to consider how the total remanence is acquired in time using nonspherical hematite particles. This is possible using our model, imposing the case when the fluid is still (no shear). Here, we neglect magnetic induction due to the particle's magnetic anisotropy. When we compare a sphere and a rotational ellipsoid of the same volume (and therefore of the same remanence) that rotate in the presence of a magnetic field, the equilibrium condition of viscous resistance to alignment is expressed by the force couples:

$$C^{sph} = 8\pi\mu r^3\omega \tag{13}$$

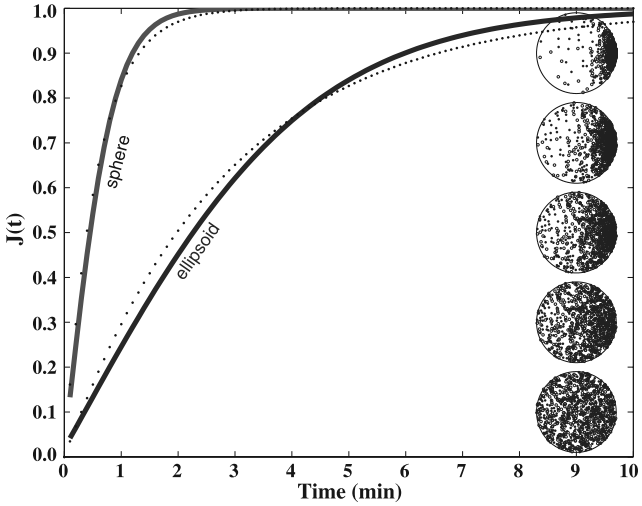

Figure 7. Evolution in total remanence (J_T) computed for 1000 initially randomly distributed, noninteracting spherical and oblate ellipsoidal particles falling in a stagnant water column. Solid curves follow equations (2) and (3), while dotted curves follow equation (16). J_T is normalized relative to the remanence value when all grains of the specified shape are aligned perfectly parallel to the field (where J_T is equal to 1). Stereonets on the right side show the distribution of the magnetic vectors at five different J_T values (0.1, 0.3, 0.5, 0.7, and 0.9).

for a sphere and

$$C^{ell} = \frac{16\pi\mu(a^2+b^2)}{3(a^2\alpha_0 + b^2\beta_0)}\omega \tag{14}$$

for an ellipsoid, where r is the sphere's radius and ω is the angular velocity. The different responses between spheres and ellipsoids may be assessed by a ratio of their couples:

$$R_{es} = \frac{C^{el}}{C^{sph}} = \frac{2(a^2+b^2)}{3abc(a^2\alpha_0 + b^2\beta_0)}. \tag{15}$$

For an oblate ellipsoid of axial ratio 1:10 that rotates about its short (c) axis, R_{es} ~5.8; when rotating around an axis in the basal plane (a = b), R_{es} ~6.7. However, equations (13) and (14) disregard the instantaneous orientation of the magnetic grain with respect to the field, and the observed remanence is produced by superposition of an assemblage of grains that are oriented differently with respect to the magnetic field. We therefore simulated multigrain systems (spheres and ellipsoids) starting from random initial orientations and found that a value of R_{es} ~5 is representative for oblate ellipsoids with an axial ratio 1:10. This means that oblate ellipsoids of axial ratio 1:10 are aligned by the magnetic field about five times slower than spheres and also that the bulk intensity of an assemblage of ellipsoids increases five times slower than for spheres.

[25] Figure 7 shows a numerical simulation of the temporal evolution in total remanence, J(t), computed for a system initially composed of 1000 randomly oriented spherical particles and oblate ellipsoids (1:10) in water with H = 50 μT. The vertical axis of Figure 7 is J(t) as a percentage of the maximum possible value, e.g., when all particles are aligned parallel to the field. Stereonet plots on the right of Figure 7 demonstrate an increase in the concentration of the remanence vectors of individual particles at a given remanence. After being exposed to a magnetic field for 0.5 min, which corresponds to the relaxation time (τ) for spheres as used in TK84, spheres attain about 50% of the maximum possible remanence following equation (13). Perfect alignment is reached at about two minutes. The remanence curve for oblate particles goes five times slower. As the evolution in total remanence [J(t)] will be used in subsequent analyses of the problem, it is convenient to approximate it by an analytic expression. For our purpose, we find a rough but mathematically simple approximation

$$J(t) = 1 - e^{-\frac{t}{q\tau}}, \tag{16}$$

where, q equals 1 for spheres and 5 for ellipsoids, as represented by the dotted curves in Figure 7.

6.3. Simultaneous Sedimentation and Alignment

[26] Settling time varies for different particle sizes and shapes. To estimate settling velocity, *Tauxe and Kent* [1984] used *Komar*'s [1980] formula for a falling disc. Combined with the well-known Stoke's law [*Happel and Brenner*, 1983, p. 231] to obtain the settling velocity means that oblate ellipsoids with an axial ratio of 1:10 fall about twice as slow as spheres of the same volume. The vertical scale on the right of Figure 8 compares the settling velocities for spheres and for ellipsoids using Stokes' equation and for discs following *Komar* [1980], with all particles being of the same volume. The scale on the left shows the time (t_b) needed for a particle to settle to the bottom through a 15 cm column of water (the tube height in the TK84 experiments). The curves are hyperbolic and the time to reach the bottom for particles with small diameters increases dramatically. Particles with D = 4 μm that were initially in the upper part

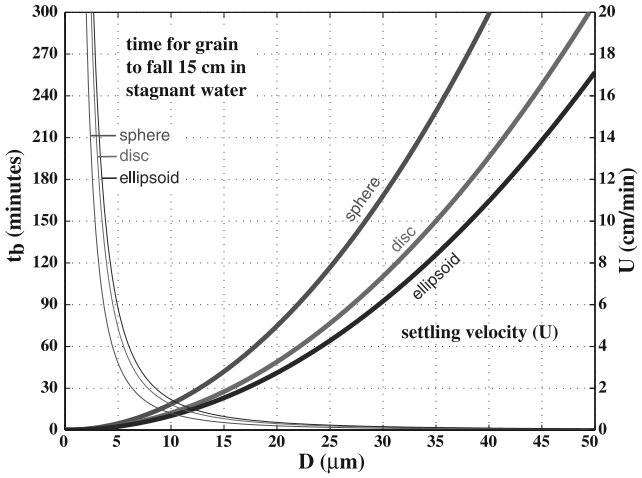

Figure 8. Settling velocity (U) for spheres, discs and ellipsoids of diameter or length (D) (thick lines) and the time (t_b) (in minutes) needed for a particle to settle 15 cm in a stagnant water column (thin lines).

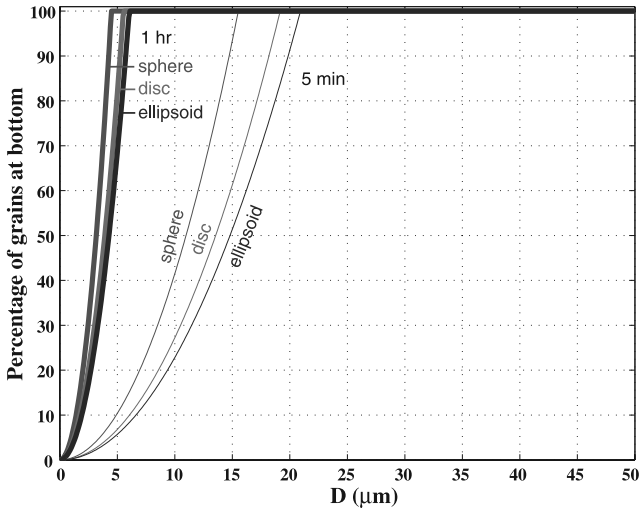

Figure 9. Fraction of particles sedimented at the bottom of the cylinder after 5 min (thin lines) and after 1 hour (thick lines) for particles of diameter (D).

of the tube require 137 min to reach the bottom. However, for smaller grains (D = 3, 2 and 1 μm) the settling time is much higher (4, 9 and 36 hours, respectively). Given the fact that TK84 observed clear water after 5 hours, it seems that the clay fraction was either composed of particles whose diameters were not much smaller than 4 μm and/or the smallest particles flocculated, and therefore they fell faster than suggested when using the Komar and Stokes equations.

[27] Figure 9 shows the fraction of particles of a given diameter that can be sedimented after 5 and 60 min, assuming an initially random particle distribution. After 5 min, almost all particles of D > 20 μm are deposited, whereas only about 20% of the particles with D $\approx$ 10 μm have fallen. After 1 hour, all particles of D > 6 μm have fallen to the bottom, but only 44% of those D $\approx$ 4 μm are sedimented, with the remaining fraction still in the column.

[28] An assessment of simultaneous settling and aligning may be done in two ways: (a) by combining the equations for particle decent with the equations for reorientation and then apply the resultant equations to a multiparticle system, or (b) use the equations for particle decent with the time function of remanence acquisition (equation (16); Figure 7). Here we treat the latter, case b. For grains of diameter D, the time dependence on the remanence accumulated at the bottom (J_b(D, t)) can be described as an integral

$$J_b(D,t) = \int J(t)\frac{U(D)}{h}dt$$

that leads to the expression

$$J_b(D,t) = \begin{cases} t_b^{-1}\int_0^t J(t)dt & t \le t_b \\ t_b^{-1}\int_0^{t_b} J(t)dt & t > t_b \end{cases}, \qquad (17)$$

where t_b = h/U(D) is the time when all particles of diameter D are at the bottom, and J(t) is a function of the remanence accumulated by a system of initially randomly oriented ellipsoids that are gradually aligned by the field as they settle. Combining equations (16) and (17) we find

$$J_b(D,t) = \begin{cases} \frac{1}{t_b}\left(t + q\tau\left(e^{-\frac{t}{q\tau}} - 1\right)\right), & t \le t_b \\ \frac{1}{t_b}\left(t_b + q\tau\left(e^{-\frac{t_b}{q\tau}} - 1\right)\right), & t > t_b \end{cases} \qquad (18)$$

The remanence J_b(D,t) is normalized, being equal to one when all particles are first aligned along the field and are then sedimented, which is strictly not possible. However, small particles fall slowly with respect to their aligning times, thus their J_b values approach 1 over sufficiently long times. On the other hand, for large particles, J_b(D,t) will be much lower than 1, because they fall too fast with respect to their aligning times. Curves J_b(D,t) for different grain diameters are shown in Figure 10, which displays the magnetic intensities at the bottom of a 15-cm-high tube assuming the sediment was composed wholly of grains of diameter D.

[29] For a grain size distribution, g(D), the total remanence accumulated at the bottom is given as an integral of the sum of the particle contributions

$$J_T(t) = \int J_b(D,t)g(D)dD. \qquad (19)$$

We don't know the exact size distribution of magnetic particles in the TK84 experiments, but conditions C1, C2 and C3 provide some important restrictions. Because 1/3 of the total remanence (J_T) (e.g., the value J_T(t) at the end of 6 hours of sedimentation) is reached after only five minutes (condition C2), J_T must be strongly influenced by large grains. Further, at five minutes, these grains must almost all

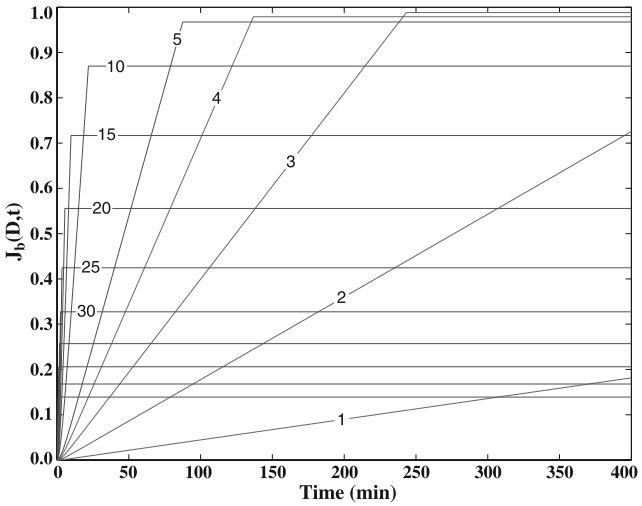

Figure 10. Time dependence on the magnetic intensity (J_b) of a sediment composed solely of a population of equal-sized grains (diameters in microns attached to the curves). J_b is measured at the bottom of a 15 cm column of water, normalized relative to the remanence value when all grains of the specified size are perfectly aligned parallel to the field.

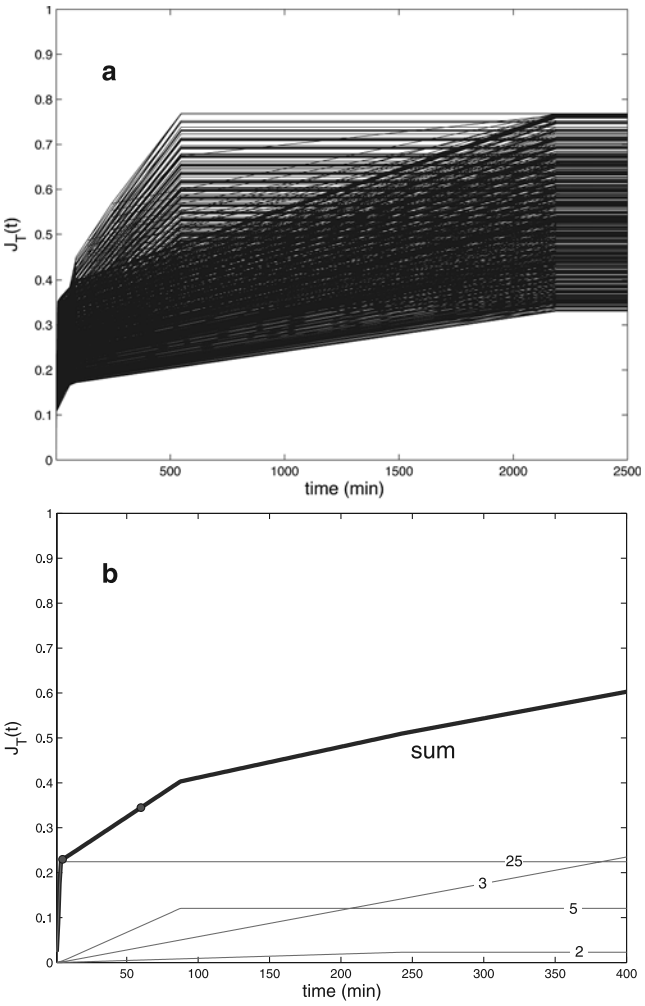

Figure 11. (a) Magnetic intensity ($J_T(t)$, normalized as in Figure 10) accumulated by four independent grain size populations, $g(D_n)$ (n = 1 to 4), where $D_1 < D_2 < D_3 < D_4$ with D ranging from 1 to 50 μm. 798 possible solutions are plotted. (b) A particular case where $D_1 = 2$, $D_2 = 3$, $D_3 = 5$ and $D_4 = 25$ μm, with $g(D_1) = 0.32$, $g(D_2) = 0.02$, $g(D_3) = 0.13$ and $g(D_4) = 0.53$, where the sum is drawn as a thick line and circles at 5 min and 1 hour indicate that conditions C2 and C3 are fulfilled.

be at the bottom because the acquisition of J_T slows down and it takes 1 hour to increase the remanence to 1/2 of J_T (condition C3). Therefore the latter stages of remanence acquisition must arise mainly from the contribution of smaller grains, with possibly some large grains that were still in the column after five minutes. In the following 5 hours, small grains continue to fall slowly to produce the other 1/2 of J_T.

[30] Equation (19) enables one to test various size distributions and choose among those that would be plausible. Consider a sediment that is composed only of four distinct grain size populations, $D_1 < D_2 < D_3 < D_4$, that have unknown relative contributions to the remanence $g(D_1)$, $g(D_2)$, $g(D_3)$, and $g(D_4)$, respectively. Grain sizes are represented by whole numbers ranging from 1 to 50 μm, e.g., D_1 is greater or equal to 1 μm and D_4 does not exceed 50 μm. Then, for any combination of grain sizes, we can derive a set of equations that corresponds to the four unknown particle distributions contributing to the remanence that satisfy conditions C1 to C3. For instance, the clay fraction ($D \leq 4$ μm) can be represented by a single population, say D_1, with D_2 to D_4 being ≥ 4 μm. Or, the clay fraction can be separated into two or three (maximum) populations, with larger grains occupying the remaining populations. For the first case we have equations,

$$\begin{aligned}
&J_b(D_1,t_b)g(D_1) = J_b(D_2,t_b)g(D_2) + J_b(D_3,t_b)g(D_3) \\
&\qquad + J_b(D_4,t_b)g(D_4), \\
&J_b(D_1,5)g(D_1) + J_b(D_2,5)g(D_2) + J_b(D_3,5)g(D_3) \\
&\qquad + J_b(D_4,5)g(D_4) = \frac{2}{3}J_b(D_1,t_b)g(D_1), \\
&J_b(D_1,60)g(D_1) + J_b(D_2,60)g(D_2) + J_b(D_3,60)g(D_3) \\
&\qquad + J_b(D_4,60)g(D_4) = J_b(D_1,t_b)g(D_1) \\
&g(D_1) + g(D_2) + g(D_3) + g(D_4) = 1
\end{aligned} \tag{20}$$

with time (5 and 60) in minutes. Similar equations can be assembled for all possible configurations of grain sizes (not all written here). Solving these equations, we found a total of 798 solutions for all potential grain sizes distributions, neglecting cases when one of the relative contributions to the remanence $g(D_1)$, $g(D_2)$, $g(D_3)$ or $g(D_4)$ was less than 0.01. The range of all solutions is shown in Figure 11a, while Figure 11b demonstrates a particular solution of four grain sizes $D_1 = 2$, $D_2 = 3$, $D_3 = 5$ and $D_4 = 25$ μm, with $g(D_1) = 0.32$, $g(D_2) = 0.02$, $g(D_3) = 0.13$ and $g(D_4) = 0.53$.

[31] An important property of the solutions is that they are additive, i.e., they combine linearly to fulfill conditions C1 to C3, meaning that there is an infinite amount of combinations from which one could construct a theoretical grain size distribution of a given sediment. Here, we use only a common feature of all solutions, where the relative value of the total remanence at the end of sedimentation lies between 0.33 and 0.77 (i.e., 33% and 77% of maximum possible alignment of hematite grains). No grain size

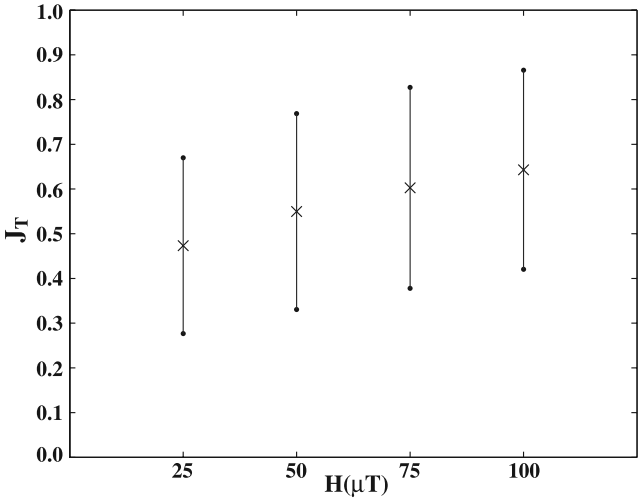

Figure 12. Mean values (crosses) and range of J_T as a function of applied field (H) that satisfy the 798 solutions in Figure 11a.

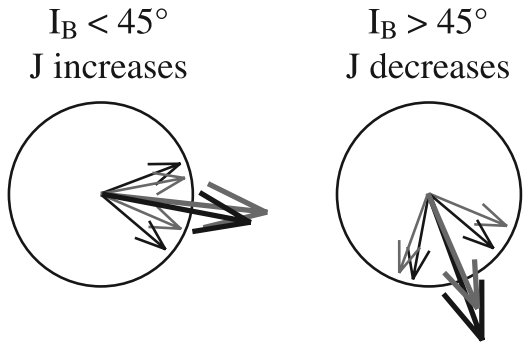

Figure 13. Simple two-dimensional model explaining why J_T (large gray arrows) varies as a function of applied field inclination (I_B) during compaction. Large black arrows represent the initial (precompaction) J_T values. Small black and gray arrows represent the theoretical range in inclination of various particles (cone about J_T) before and after compaction, respectively. When $I_B < 45°$, the spread about the mean decreases, which increases J_T. When $I_B > 45°$, the spread about the mean increases, which decreases J_T.

distribution fulfills conditions C1 to C3 when the bottom total remanence at the end of the aligning process is above 0.77. We used all 798 solutions to simulate J_T for field values of 25, 50, 75 and 100 μT, with the mean and range shown in Figure 12, which are representative of the recorded remanence from free alignment until the grains hit the bottom. The mean values reflect the dependence of J_T on H and are used in subsequent analyses. We emphasize that until now we have neglected grain-to-grain interaction during falling, flocculation and mechanical interaction at the bottom, all of which would lead to randomization and hence to decrease the remanence.

6.4. Shallowing

[32] When grains sediment gradually, they hit the bottom, rotate to a final position and are overlain by subsequent grains. The layer then slowly compacts under the weight of the overlying grains. All these effects likely act to shallow the recorded inclination (I_r) in the rock with respect to the field inclination (I_B) [*King*, 1955; *Løvlie and Torsvik*, 1984; *Arason and Levi*, 1990; *Borradaile*, 1993]. Without information about the size distribution of the grains in the sediment (both magnetic and nonmagnetic), it is hard to model the shallowing process. On the other hand, we can use the relationship $\tan(I_r) = F \times \tan(I_B)$, where F is commonly between 0.3 and 0.6 (0.55 in TK84). A rock exhibiting inclination shallowing contains many grains that were differentially reoriented toward and away from the field direction. A simplified way to model the shallowing process is to consider that every grain undergoes equal amounts of reorientation, and then select a value corresponding to this effective grain reorientation that reproduces the observed inclination error.

[33] To complete this step, we take a multigrain system, already modeled in the aligning phase of sedimentation, and then reorient each grain such that the net inclination is lowered to a value corresponding to $F = 0.55$. This is achieved by multiplying the direction cosines of all the individual grains by a matrix,

$$\mathbf{M} = \begin{bmatrix} 1 & 0 & 0 \\ 0 & 1 & 0 \\ 0 & 0 & \theta \end{bmatrix}, \tag{21}$$

which may be applied gradually as the particles enter the lowest part of the tube during sedimentation, or simulta-

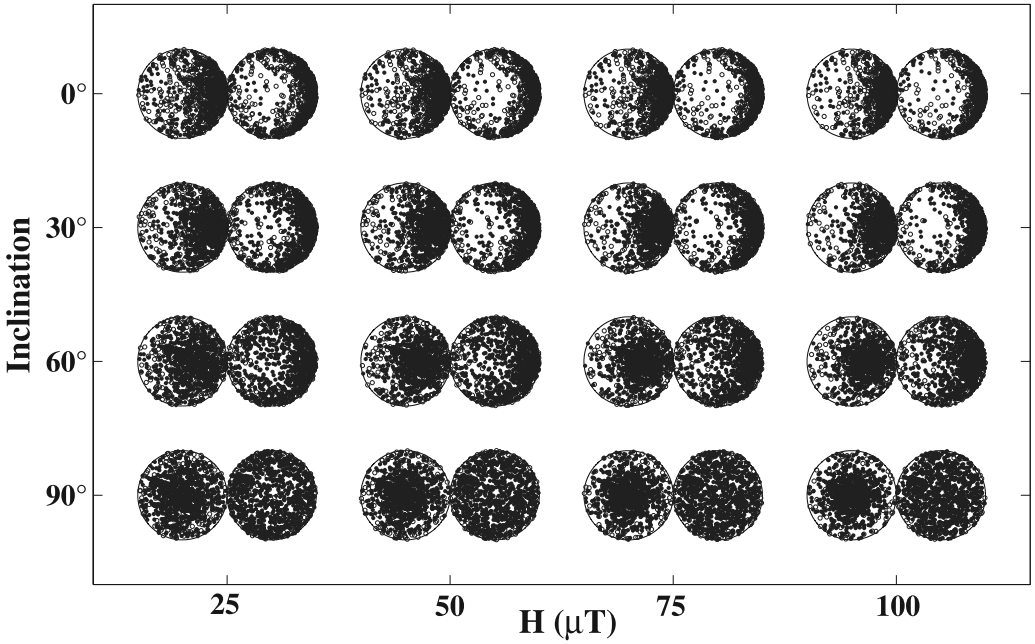

Figure 14. Stereonets showing the directions of 1000 individual particles oriented under specified conditions of applied field inclination and intensity. Stereonets to the left of each pair correspond to the state after settling yet before compaction. Those on the right are after settling and after compaction.

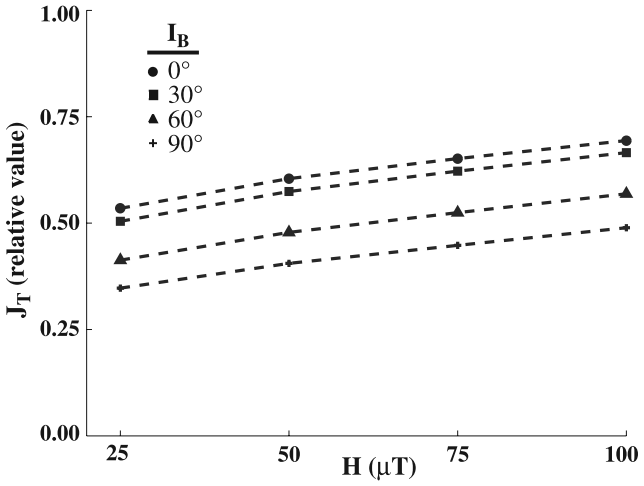

Figure 15. Total remanence (J_T) after inclination shallowing under specified applied fields (H) as a function of applied field inclination (I_B).

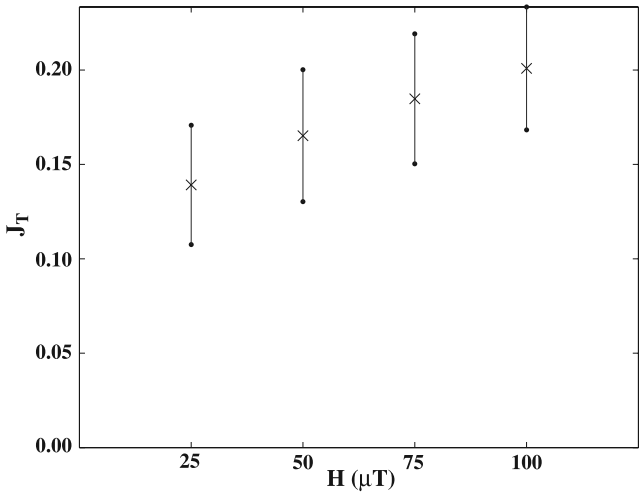

Figure 17. Mean values (crosses) and range of total remanence (J_T) as a function of applied field (H) after simulating flocculation (see Figure 12 for comparison).

neously to all particles at the end of settling. The magnitude of grain reorientation on J_T depends on I_B. If I_B is < 45°, J_T increases; if I_B > 45°, J_T decreases (Figure 13). On the other hand, the magnitude of shallowing (I_r/I_B) is independent of J_T. In order to estimate θ, we matched resulting I_r/I_B versus H against the curves from TK84, which yields θ of 0.4 to 0.5.

[34] Figures 14, 15, and 16 illustrate the application of equation (21) to a multigrain system (1000 grains) for combinations of field intensities H = 25, 50, 75, and 100 μT and field inclinations I_B = 0°, 30°, 60°, and 90° (J_T from Figure 7 corresponds to 0.47, 0.55, 0.60, and 0.64). Figure 14 shows two stereonets for each combination of I_B and H. The left one corresponds to the case after settling yet before shallowing, and the right one is after settling and after shallowing. When considering J_T after shallowing, one finds a robust correlation between J_T, H and I_B (Figure 15). Although the curves of J_T as a function of I_B and H from our model are less steep, they show similar dispersion of J_T with respect to H as those from the TK84 experiments. Figure 16 confirms that the numerical procedure we used to model shallowing exhibits almost no dependence on field intensity and that I_r/I_B ratios are similar to those of the TK84 experiments.

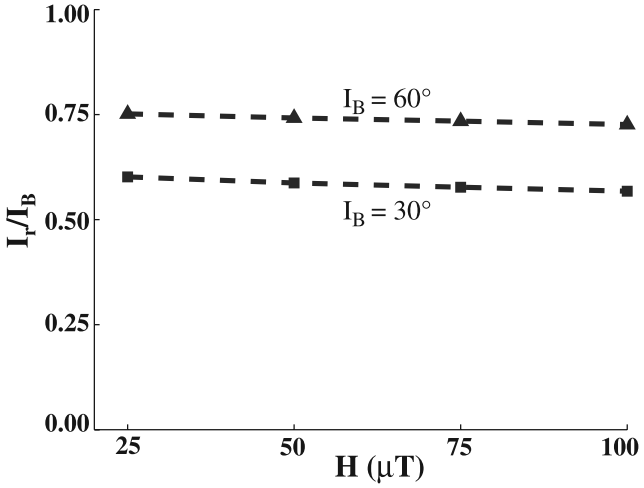

Figure 16. Inclination shallowing (I_r/I_B) versus field intensity (H) showing relative independence between the two for I_B of 30° and 60°.

6.5. Flocculation

[35] *Tauxe and Kent* [1984] tried to avoid flocculation in their experiments by using deionized water, but the flocculation of small grains is difficult to eliminate, especially when considering that the water in the redeposition columns was clear after only 5 hours. Also, the fall velocities and the time for the smallest grains to reach the bottom (Figure 8) indicate that there should be some flocculation taking place. To examine possible flocculation effects on remanence acquisition, one needs to know how the flocs grow in time. A simplified scenario considers that hematite grains attach to spherical flocs [*Katari and Bloxham*, 2001]. The density of the flocs would be similar to clay, which together with their spherical shape, would change the fall velocity and the alignment time. This also changes the effective volumetric J_V. Moreover, it seems plausible to allow the hematite grains to be initially free to align for a short period before they become attached to flocs, i.e., the phases of aligning then flocculation and settling are delayed. For settling with flocculation, the above equations and procedures are again valid.

[36] We examined different flocculation scenarios by varying floc size, the sizes of hematite grains allowed to flocculate, and the times for the hematite grains to rotate freely before flocculating. For example, Figures 17 and 18a show simulations of hematite grains that aligned freely for two minutes before becoming flocculated. Only hematite grains D $\leq$ 6 μm were allowed to flocculate and they adhered to particles of 13 μm, which is the mean sediment grain size in TK84. The percentage of hematite grains that flocculate depend on their sizes, with 90% of the grains D = 1 μm being able to flocculate (e.g., 10% did not flocculate and freely rotated throughout the allotted time),

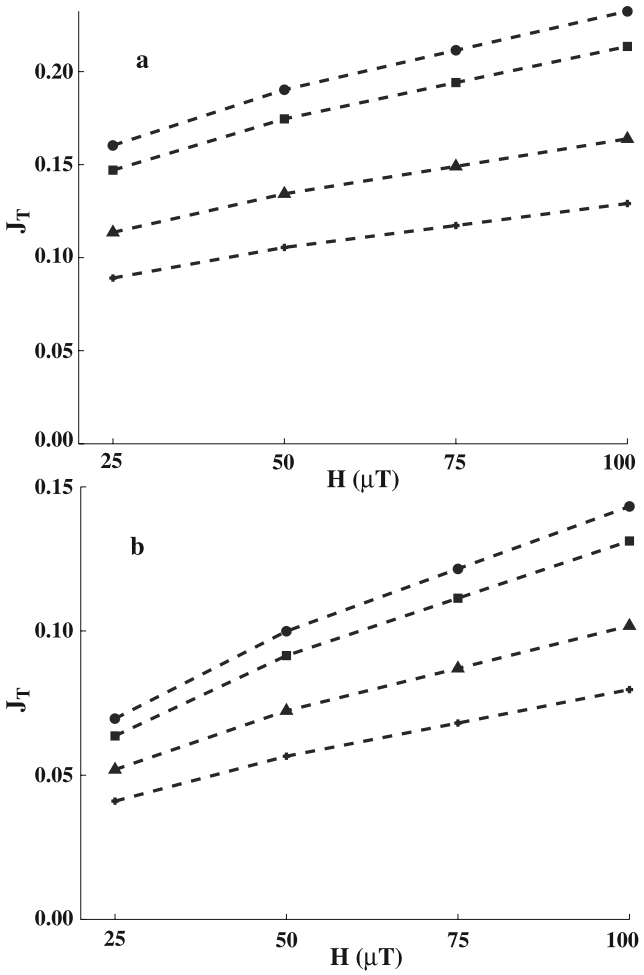

Figure 18. (a) Total remanence (J_T) after flocculation and compaction under specified applied fields (H) as a function of applied field inclination (I_B). (b) Same as in Figure 18a except that the mean J_T was decreased from 3/30 to 1/30 to match the experimental data.

and similarly 85, 80, 70, 50, and 30% of the grains with D = 2,..,6 μm become incorporated into flocs (6 μm being the cutoff size for flocculating hematite grains). The general effects of flocculation are faster accumulation rates and lower J_T, and that the pattern of J_T(H) is similar as in Figure 12. Figure 18a again demonstrates the sensitivity of the final J_T with both field intensity and inclination.

6.6. Mechanical Interaction and Summary of Modeling the TK84 Experiments

[37] The curves in Figures 15 and 18a show a dispersion of J_T with respect to H and I_B, but their slopes are shallower than in TK84. A possible explanation could be that the grain or floc orientations in the redeposition experiments become partly randomized due to mutual interactions during fall and when hitting bottom. The randomization would decrease J_T in the following manner. For applied fields of 25 μT with any inclination, TK84 found that the minimum value of J_T is 1×10^{-5} A m^2 kg^{-1}. The saturation experiments on page 551 of TK84 show a maximum possible J_T of about 30×10^{-5}. Therefore the values recorded during the experiments were 1/30 of the possible maximum. In Figure 17, the minimum mean J_T value that was used for modeling Figure 18a was about 0.1 (or 3/30); that is, we reached a higher recorded remanence than that of the experiments. By assuming that randomization would decrease the J_T recorded during the settling and aligning steps (Figure 17), such that the minimum value of 0.1 was diminished from 3/30 to 1/30, the mean J_T values decrease. When we then apply the shallowing step, the curves become steeper and the pattern more closely resembles that observed by TK84 (Figure 18b).

[38] The extent that a numerical model can explain experimental results is questionable, especially given the lack of known parameters inherent in the experiments themselves. Despite this, we have shown that a viscous model can successfully explain, at least in rough approximation, one set of data that contains a minimum of critical information regarding the grain size distribution of the particles that carry the magnetic remanence and the field dependence on inclination and remanent intensity. This suggests that our viscous model can lend insight into the process of remanence acquisition in sediments. This conclusion runs opposite to that of *Tauxe and Kent* [1984] whose data we used. The differences are based on the fact that our approach accounts for the time dimension on aligning a population of multiple particles and for the differences in the orientation processes between ellipsoids and spheres. Because of these differences, we find that a proportion of hematite grains in the TK84 investigations cannot have become completely aligned with the applied field direction. Nonideal alignment, together with shallowing, modifies the final recorded magnetic remanent intensity of the sediment, which varies with respect to the applied field intensity and the applied field inclination. Inclination shallowing is largely independent of field intensity. Our treatment suggests that factors such as grain-to-grain interactions, flocculation, etc., must be added to more closely mimic the TK84 results. Note that the sediments and the relatively rapid timescales used in the TK84 experiments are more similar to those found in the continental environment. Extrapolating the findings herein to other situations, such as the marine environment [*Katari et al.*, 2000], will require further reflection. Future redeposition experiments that can provide better knowledge of the size and shape distributions of magnetic and nonmagnetic particles, and how they contribute to the bulk remanence in time, will further improve the applicability of viscous models to different sedimentary conditions.

7. Magnetic Anisotropy

[39] For completeness, we briefly mention that our model can also calculate magnetic anisotropies of multiparticle systems and we can simultaneously model the development of both remanence (direction and intensity) and magnetic fabric (principal susceptibility axis directions, degree of anisotropy, etc). Preliminary examples in Figure 19 show two scenarios of the time evolution of a distribution of hematite particles in a fluid of viscosity 10^3 Pa s. Shear is turned off, e.g., no external shear is applied so the magnetic grains are oriented solely by the magnetic field; time (t) is in months. In the first case (Figure 19, top), the particles are

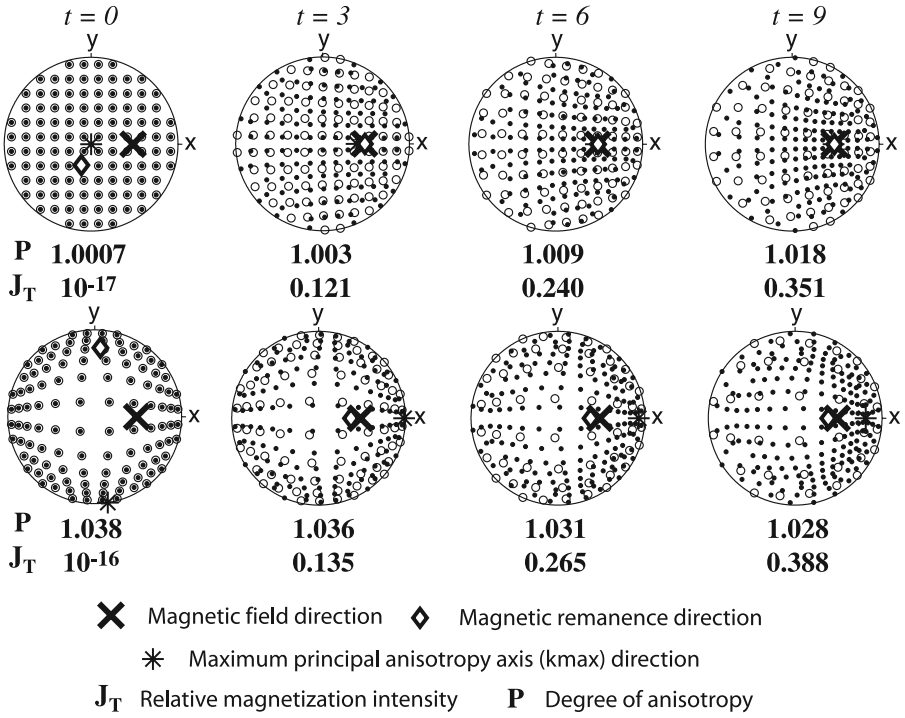

Figure 19. An example of the development of remanence and magnetic susceptibility in a multiparticle system of hematite grains in a fluid of viscosity 10^3 Pa s that are oriented solely by the magnetic field; time (t) is in months. (top) With particles starting from an initially isotropic distribution, both the remanence direction and the maximum principal susceptibility axis are simultaneously aligned parallel to the magnetic field. (bottom) If the particles are first compacted, then the remanence direction orients parallel to the field while the maximum principal susceptibility axis lies in the bedding plane. With time, the latter will gradually approach the field direction.

initially isotropically distributed (zero remanence and no anisotropy of magnetic susceptibility (AMS)), and then both the remanence direction and the maximum principal susceptibility axis are progressively aligned parallel to the magnetic field. In Figure 19 (bottom), we first compacted the particles along the *z* axis (which simulates the compaction of a horizontal sedimentary layer), then turned on the field. Figure 19 (bottom) shows that the model can achieve what is found in nature, a remanent inclination that approaches the field value and a bedding-parallel magnetic foliation.

8. Conclusions

[40] Although our model contains some assumptions (slowly moving Newtonian fluid, noninteracting, rigid, ellipsoidal particles) that may not be strictly valid in nature, it does provide a reference frame for studying the motion of magnetic particles simultaneously subjected to magnetic and hydrodynamic forces. It allows one to observe how (or if), and under what timescales, magnetic particles immersed in fluids of variable viscosity would orient in the influence of an external magnetic field. As it covers ellipsoidal particles, the model represents an advance over spherical approximations.

[41] The analyses of the governing equations show how, in fluids of equal viscosity, longer times are required for hematite than for magnetite particles to orient parallel to an external field. The results could have important implications for the recording process in sediments. Because viscosity increases with depth in dense slurries, particles deposited under conditions of high sedimentation rates will have less time to reorient then under slow rates. Moreover, in creeping/flowing fluids, flow direction can influence the ultimate inclination recorded by the particle. Thus the magnetic directions of particles deposited on slopes, such as on a deltaic fan or in the continental environment, may be systematically deviated from the true field direction, with differences of 10° being within the realm of geologically plausible conditions.

[42] Probably the single-most important flaw in the discipline of paleomagnetism is accurately determining geomagnetic field inclination in sediments. Because paleolatitude is calculated directly from inclination, aberrations in the recording process of magnetic inclination lead to erroneous estimates of latitudinal transport. Shallow paleolatitudes pose a particular dilemma in central Asia, where unrealistic amounts of poleward translations are implied [*Gilder et al.*, 2001]. Dominating the central Asian landscape are the Tianshan Mountains, which trend E-W over a distance of 2500 km. Sediments shed from the Tianshan are transported via a network of north or south flowing rivers and then deposited in two large intracontinental basins flanking the range. The sediments deposited near the Tianshan in those basins thus provide an ideal natural case to test our results.

[43] Magnetostratigraphy of two Neogene sections located on both sides of the Tianshan Mountains show that the Yaha section, located on the southern flank of the Tianshan, has a much shallower mean inclination (43°) than the mean inclination from the Kuitun section from the northern flank (57°) [*Charreau et al.*, 2005, 2006]. The geocentric axial dipole field inclination at the site and the expected inclination from the 10 or 20 Ma reference poles from the Eurasian apparent polar wander path are all on the order of 62°; thus much more in agreement with Kuitun than Yaha. If the differences between the northern and southern flanks were interpreted in a classical tectonic framework, then the Tianshan Mountains would have accommodated >1000 km of shortening in the past 5 million years. This is clearly impossible. On the other hand, if one understands why the difference exists between the northern and southern flanks, one can better understand the mechanism resulting in the inclination differences.

[44] The observed inclination values from the Tianshan region can be used to test our numerical results. If the lock in of magnetic remanence occurred while the sediments were slowly creeping on slopes, then the shear component arising from the hydrodynamic couple would contribute to the lock-in process and result in shallower inclinations on the south dipping slopes at Yaha than on the north dipping slopes at Kuitun. Higher average sedimentation rates at Yaha (∼30 cm/kyr) than at Kuitun (∼20 cm/kyr), would also contribute to shallower inclinations at Yaha because greater viscosities from increased sediment loads diminish reorientation times. Moreover, magnetite carries the magnetic remanence in Kuitun while hematite carries the magnetic remanence in Yaha, thus the magnetic couple is stronger at Kuitun than at Yaha. Although it is premature to quantify the effects of each of the three processes, creep, reorientation time (viscosity) or magnetic couple, creep can likely be discounted because the majority of the studied rocks yield shallow inclinations, whereas the slopes in central Asia dip on average to the north due to the northward propagation of India as it penetrates Asia. This would lead to steeper inclinations on average, which is not the case. At Yaha, sedimentation rate increases from 20 to 43 cm kyr^{-1} [*Charreau et al.*, 2006], yet the recorded inclinations do not change. This suggests that reorientation must occur at the higher levels of sedimentation, because the viscosity profile in thick deposits should be steeper than that in thin ones. Of the three possibilities, magnetic couple thus seems the most important because the majority of Upper Jurassic to present red beds throughout central Asia have shallow inclinations and their magnetizations are carried by hematite. To our knowledge, besides Kuitun, the only other study of central Asian sediments (Yumen area) whose remanence is carried by magnetite does not have significantly shallow inclinations [*Chen et al.*, 2002]. However, at Yaha and at Subei [*Gilder et al.*, 2001], both magnetite and hematite are identified in the sediments but the magnetization directions at 500°C (well below the Curie temperature of magnetite) are the same as at 600°C (above the Curie temperature of magnetite), implying that magnetite and hematite record the same direction. More detailed knowledge on the magnetic recorders and how their remanence directions are fixed in the sediments is clearly needed.

[45] In the future, we hope to apply the model developed herein to empirical data by including the time evolution of preferred orientations in multiparticle systems and corresponding magnetic remanence. This will enable one to better understand the evolution of remanent magnetization and magnetic fabric in sedimentary rocks, and permits one to explore how the flocculation process will influence field recording in sediments. Our model will allow us to explore more complicated cases with combinations of pure and simple shear to simulate compaction acting during sedimentation.

Appendix A

[46] Consider that an ellipsoidal magnetic particle has rotational symmetry. For a prolate particle with semiaxes $a > b = c$, we can evaluate the integrals

$$\alpha_0 = \int_0^\infty \frac{d\lambda}{(a^2+\lambda)^{3/2}(b^2+\lambda)} = \frac{2}{(a^2-b^2)^{3/2}} \cdot \left\{ \frac{1}{2}\log\frac{a+\sqrt{a^2-b^2}}{a-\sqrt{a^2-b^2}} - \sqrt{\frac{a^2-b^2}{a^2}} \right\}$$

$$\beta_0 = \int_0^\infty \frac{d\lambda}{(a^2+\lambda)^{1/2}(b^2+\lambda)^2} = \frac{1}{(a^2-b^2)^{3/2}} \cdot \left\{ \frac{\sqrt{a^2(a^2-b^2)}}{b^2} - \frac{1}{2}\log\frac{a+\sqrt{a^2-b^2}}{a-\sqrt{a^2-b^2}} \right\}.$$

For an oblate particle with $a < b = c$,

$$\alpha_0 = \int_0^\infty \frac{d\lambda}{(a^2+\lambda)^{3/2}(b^2+\lambda)} = \frac{2}{(b^2-a^2)^{3/2}} \cdot \left\{ \sqrt{\frac{b^2-a^2}{a^2}} - arctg\sqrt{\frac{b^2-a^2}{a^2}} \right\}$$

$$\beta_0 = \int_0^\infty \frac{d\lambda}{(a^2+\lambda)^{1/2}(b^2+\lambda)^2} = \frac{1}{(b^2-a^2)^{3/2}} \cdot \left\{ arctg\sqrt{\frac{b^2-a^2}{a^2}} - \frac{\sqrt{a^2(b^2-a^2)}}{b^2} \right\}.$$

Some values of these parameters are in Table A1. To find the values for real particle dimensions we note that if all the semi axes are multiplied by a factor d, parameters α_0 and β_0 change by d^{-3}.

Appendix B

[47] For the situation in Figure 2, equations (7) simplify to

$$\omega_1 = \omega_3 = 0, \quad \text{and}$$

$$\omega_2 = \frac{c^2 - a^2}{c^2 + a^2} E_{13} - \Omega_{13} + \frac{3(c^2\gamma_0 + a^2\alpha_0)}{16\pi\mu(c^2+a^2)} C_2^M.$$

Table A1. Parameters α_0, and β_0 for Different Aspect Ratios

	Prolate Particle, a = R, b = c = 1		Oblate Particle, a = 1, b = c = R	
Aspect Ratio R	α_0	β_0	α_0	β_0
1	2/3	2/3	2/3	2/3
2	0.174	0.413	0.264	0.118
3	0.072	0.297	0.141	0.041
4	0.038	0.232	0.088	0.019
5	0.022	0.189	0.060	0.010
10	0.004	0.098	0.017	0.001

In a coordinate system fixed in space, the velocity gradient tensor for simple shear is

$$L_{ij} = \begin{pmatrix} 0 & 0 & 0 \\ 0 & 0 & 0 \\ -\gamma & 0 & 0 \end{pmatrix},$$

and its symmetric and asymmetric parts are

$$E_{ij} = \begin{pmatrix} 0 & 0 & -\gamma/2 \\ 0 & 0 & 0 \\ -\gamma/2 & 0 & 0 \end{pmatrix}, \qquad \Omega_{ij} = \begin{pmatrix} 0 & 0 & \gamma/2 \\ 0 & 0 & 0 \\ -\gamma/2 & 0 & 0 \end{pmatrix}.$$

The rotation matrix describing the relationship between a fixed coordinate system and a coordinate system rotating with particle is

$$R_{ij} = \begin{pmatrix} \cos\varphi & 0 & -\sin\varphi \\ 0 & 1 & 0 \\ \sin\varphi & 0 & \cos\varphi \end{pmatrix},$$

where $\varphi = I_B + \delta$. Expressing the symmetric and asymmetric part of the velocity gradient tensor in the rotating system leads to

$$E_{ij} = R_{ik}R_{jl}E'_{kl}, \quad \Omega_{ij} = R_{ik}R_{jl}\Omega'_{kl} \quad ,$$

$$E_{13} = -\frac{\gamma}{2}(R_{11}R_{33} + R_{13}R_{31}) = -\frac{\gamma}{2}\left(\cos^2\varphi - \sin^2\varphi\right) = -\frac{\gamma}{2}\cos 2\varphi \quad ,$$

$$\Omega_{13} = \frac{\gamma}{2}(R_{11}R_{33} - R_{13}R_{31}) = \frac{\gamma}{2}\left(\cos^2\varphi + \sin^2\varphi\right) = \frac{\gamma}{2}$$

and for the magnetic force couple,

$$C_1^M = C_3^M = 0 \quad \text{and} \quad C_2^M = VJ_VB\sin\delta = \frac{4}{3}\pi abcJ_VB\sin\delta.$$

After completing the equation for angular velocity we obtain

$$\omega_2 = -\frac{c^2 - a^2}{c^2 + a^2}\frac{\gamma}{2}\cos 2(I_B + \delta) - \frac{\gamma}{2} + \frac{abc(c^2\gamma_0 + a^2\alpha_0)}{4(c^2 + a^2)}\frac{J_VB}{\mu}\sin\delta.$$

For the situation in Figure 2, the angular velocity of particle rotating in the x-z plane is $\omega = \delta = -\omega_2$.

[48] Substituting further the values for $a = 2$, $b = c = 1$, $\alpha_0 = 0.174$, $\beta_0 = \gamma_0 = 0.413$ (see Table A1), we obtain equation (9a). Equation (9b) has only a reversed sign in simple shear terms.

[49] Note that if there is no flow ($\gamma = 0$) and the particle is a sphere, the last equation may be written

$$\frac{d\delta}{dt} = -\frac{J_VB}{6\mu}\sin\delta$$

and solved as

$$\tan\left(\frac{\delta}{2}\right) = \tan\left(\frac{\delta_o}{2}\right)e^{-\frac{J_VB}{6\mu}t},$$

which corresponds to the solution for spherical magnetic particles in a viscous fluid as given by *Nagata* [1961].

[50] **Acknowledgments.** This contribution was supported by the Czech Grant Agency (grant 205/03/0336) and through the invited professorship program (to J.J.) from the University of Paris VII (Denis Diderot) and the Institut de Physique du Globe de Paris. We thank Graham Borradaile, Mike Jackson, Ken Kodama, Reidar Løvlie, and an anonymous reviewer for helpful comments and suggestions. IPGP contribution 2159.

References

Anson, G. L., and K. P. Kodama (1987), Compaction-induced inclination shallowing of the post- depositional remanent magnetization in a synthetic sediment, *Geophys. J. R. Astron. Soc.*, *88*, 673–692.

Arbaret, L., A. Fernandez, J. Jezek, B. Ildefonse, P. Launeau, and H. Diot (2000), Analogue and numerical modelling of shape fabrics: Application to strain and flow determination in magmas, *Trans. R. Soc. Edinburgh Earth Sci.*, *90*, 97–109.

Arason, P., and S. Levi (1990), Models of inclination shallowing during sediment compaction, *J. Geophys. Res.*, *95*, 4481–4499.

Borradaile, G. (1993), Strain and magnetic remanence, *J. Struct. Geol.*, *15*, 383–390.

Charreau, J., Y. Chen, S. Gilder, S. Dominguez, J. P. Avouac, S. Sen, D. J. Sun, Y. A. Li, and W. M. Wang (2005), Magnetostratigraphy and rock magnetism of the Neogene Kuitun He section (northwest China): Implications for Late Cenozoic uplift of the Tianshan mountains, *Earth Planet. Sci. Lett.*, *230*, 177–192.

Charreau, J., S. Gilder, Y. Chen, S. Dominguez, J. P. Avouac, S. Sen, M. Jolivet, Y. A. Li, and W. M. Wang (2006), Magnetostratigraphy of the Yaha section, Tarim Basin (China): 11 Ma acceleration in erosion and uplift of the Tianshan Mountains, *Geology*, *34*, 181–184.

Chen, Y., H. N. Wu, V. Courtillot, and S. Gilder (2002), Large NS convergence at the northern edge of the Tibetan Plateau? New Early Cretaceous paleomagnetic data from Hexi Corridor, NW China, *Earth Planet. Sci. Lett*, *201*, 293–307.

Collinson, D. W. (1965), The remanent magnetization and magnetic properties of red sediments, *Geophys. J. R. Astron. Soc.*, *10*, 105–126.

Collinson, D. W. (1983), *Methods in Rock Magnetism and Palaeomagnetism: Techniques and Instrumentation*, 503 pp., CRC Press, Boca Raton, D. C.

Deamer, G. A., and K. P. Kodama (1990), Compaction-induced inclination shallowing in synthetic and natural clay-rich sediments, *J. Geophys. Res.*, *95*, 4511–4529.

Debat, P., P. Sirieys, J. Deramond, and J. C. Soula (1975), Paleodéformations d'un massif orthogenessique (massif des Cammazes. Montagne Noire Occidentale. France), *Tectonophysics*, *28*, 159–183.

Denham, C. R., and A. D. Chave (1982), Detrital remanent magnetization: Viscosity theory of the lock-in zone, *J. Geophys. Res.*, *87*, 7126–7130.

Fernandez, A. (1988), Strain analysis from shape preferred orientation in magmatic flows, *Bull. Geol. Inst. Univ. Uppsala*, *14*, 61–67.

Gay, N. C. (1968), The motion of rigid particles embedded in a viscous fluid during pure shear deformation of the fluid, *Tectonophysics*, *5*, 81–88.

Gilder, S., Y. Chen, and S. Sen (2001), Oligo-Miocene magnetostratigraphy and rock magnetism of the Xishuigou section, Subei (Gansu Province,

western China), and implications for shallow inclinations in central Asia, *J. Geophys. Res.*, *106*, 30,505–30,521.
Gilder, S., Y. Chen, J. P. Cogne, X. D. Tan, V. Courtillot, D. J. Sun, and Y. A. Li (2003), Paleomagnetism of Upper Jurassic to Lower Cretaceous volcanic and sedimentary rocks from the western Tarim Basin and implications for inclination shallowing and absolute dating of the M-0 (ISEA?) chron, *Earth Planet. Sci. Lett.*, *206*, 587–600.
Granar, L. (1957), Magnetic measurements on Swedish varved sediments, *Ark. Geofys.*, *3*, 1–40.
Griffiths, D. H., R. F. King, and A. I. Rees (1962), The relevance of magnetic measurements on some fine particle silts to the study of their depositional process, *Sedimentology*, *1*, 134–144.
Hamano, Y. (1980), An experiment on the post-depositional remanent magnetization in artificial and natural sediments, *Earth Planet. Sci. Lett.*, *51*, 221–232.
Hamilton, N., and R. F. King (1964), Comparison of the bedding errors of artificially and naturally deposited sediments with those predicted from a simple model, *Geophys. J. R. Astron. Soc.*, *8*, 370–374.
Hamilton, N., W. H. Owens, and A. I. Rees (1968), Laboratory experiments on the production of grain orientation in shearing sand, *J. Geol.*, *76*, 465–472.
Happel, J., and H. Brenner (1983), *Low Reynolds Number Hydrodynamics*, 572 pp., Martinus Nijoff, Zoetermeer, Netherlands.
Hrouda, F. (2002), Low-field variation of magnetic susceptibility and its effect on the anisotropy of magnetic susceptibility of rocks, *Geophys. J. Int.*, *150*, 715–723.
Ildefonse, B., L. Arbaret, and H. Diot (1997), Rigid particles in simple shear flow: Is their preferred orientation periodic or steady-state?, in *Granite: From Segregation of Melt to Emplacement Fabrics*, edited by J. L. Bouchez, pp. 159–176, Springer, New York.
Irving, E., and A. Major (1964), Post-depositional remanent magnetization in a synthetic sediment, *Sedimentology*, *3*, 135–143.
Jackson, M., G. Borradaile, P. Hudleston, and S. Banerjee (1993), Experimental deformation of synthetic magnetite-bearing calcite sandstones: Effects on remanence, bulk magnetic properties, and magnetic anisotropy, *J. Geophys. Res.*, *98*, 383–401.
Jeffery, G. B. (1922), The motion of ellipsoidal particles immersed in a viscous fluid, *Proc. R. Soc. London, Ser. A*, *102*, 161–179.
Jezek, J. (1994), Software for modelling the motion of rigid triaxial ellipsoidal particles in viscous flow, *Comput. Geosci.*, *20*, 409–424.
Jezek, J., K. Schulmann, and K. Segeth (1996), Fabric evolution of rigid inclusions during mixed coaxial and simple shear flows, *Tectonophysics*, *257*, 203–221.
Jezek, J., S. Saic, K. Segeth, and K. Schulmann (1999), Three-dimensional hydrodynamical modelling of viscous flow around a rotating ellipsoidal inclusion, *Comput. Geosci.*, *25*, 547–558.
Katari, K., and J. Bloxham (2001), Effects of sediment aggregate size on DRM intensity: A new theory, *Earth Planet. Sci. Lett.*, *186*, 113–122.
Katari, K., L. Tauxe, and J. King (2000), A reassessment of post-depositional remanent magnetism: Preliminary experiments with natural sediments, *Earth Planet. Sci. Lett.*, *183*, 147–160.
Kent, D. (1973), Post-depositional remanent magnetisation in deep-sea sediment, *Nature*, *246*, 32–34.
King, R. F. (1955), The remanent magnetism of artificially deposited sediments, *Mon. Not. R. Astron. Soc. Geophys. Suppl.*, *7*, 115–134.
King, R. F., and A. I. Rees (1966), Detrital magnetism in sediments: An examination of some theoretical models, *J. Geophys. Res.*, *71*, 561–571.
Kodama, K. P. (1988), Remanence rotation due to rock strain during folding and the stepwise application of the fold test, *J. Geophys. Res.*, *93*, 3357–3371.
Kodama, K. P., and A. G. Goldstein (1991), Experimental simple shear deformation of magnetic remanence, *Earth Planet. Sci. Lett.*, *104*, 80–88.
Kodama, K. P., and W. W. Sun (1992), Magnetic-anisotropy as a correction for compaction-caused paleomagnetic inclination shallowing, *Geophys. J. Int.*, *111*, 465–469.
Kodama, K. P., and P. D. Ward (2001), Compaction-corrected paleomagnetic paleolatitudes for Late Cretaceous rudists along the Cretaceous California margin: Evidence for less than 1500 km of post-Late Cretaceous offset for Baja British Columbia, *Geol. Soc. Am. Bull.*, *113*, 1171–1178.
Komar, P. D. (1980), Settling velocities of circular cylinders at low Reynolds numbers, *J. Geol.*, *88*, 327–336.
Løvlie, R., and T. Torsvik (1984), Magnetic remanence and fabric properties of laboratory-deposited hematite-bearing red sandstone, *Geophys. Res. Lett.*, *11*, 221–224.
Migniot, C. (1989a), Tassement et rhéologie des vases: Première partie, *Houille Blanche*, *1*, 11–29.
Migniot, C. (1989b), Tassement et rhéologie des vases: Deuxiéme partie, *Houille Blanche*, *2*, 95–111.
Nagata, T. (1961), *Rock Magnetism*, 350 pp., Mazuren, Tokyo.
Opdyke, N. D. (1971), The paleomagnetism of the New Jersey Triassic: A field study of the inclination error in red sediments, *J. Geophys. Res.*, *66*, 1941–1948.
Rees, A. I. (1961), The effect of water currents on the magnetic remanence and anisotropy of susceptibility of some sediments, *Geophys. J. R. Astron. Soc.*, *5*, 235–251.
Rees, A. I. (1964), Measurements of the natural remanent magnetism and anisotropy of susceptibility of some Swedish glacial silts, *Geophys. J. R. Astron. Soc.*, *8*, 356–369.
Rees, A. I. (1971), The magnetic fabric of a sedimentary rock deposited on a slope, *J. Sediment. Petrol.*, *41*, 307–309.
Rees, A. I. (1979), The orientation of grains in a sheared dispersion, *Tectonophysics*, *55*, 275–287.
Rees, A. I., and W. A. Woodall (1975), The magnetic fabric of some laboratory-deposited sediments, *Earth Planet. Sci. Lett.*, *25*, 121–130.
Shcherbakov, V. P., and V. V. Shcherbakov (1987), On the physics of acquisition of post-depositional remanent magnetization, *Phys. Earth Planet. Inter.*, *46*, 64–70.
Shive, P. N. (1985), Alignment of magnetic grains in fluids, *Earth Planet. Sci. Lett.*, *72*, 117–124.
Stacey, F. D. (1972), On the role of Brownian motion in the control of detrital remanent magnetization of sediments, *Pure Appl. Geophys.*, *98*, 139–145.
Sun, W. W., and K. P. Kodama (1992), Magnetic anistropy, scanning electron microscopy, and X-ray pole figure goniometry study of inclination shallowing in a compacting clay-rich sediment, *J. Geophys. Res.*, *97*, 19,599–19,615.
Tan, X., K. P. Kodama, H. Chen, D. Fang, D. Sun, and Y. Li (2003), Paleomagnetism and magnetic anisotropy of Cretaceous red beds from the Tarim basin, northwest China: Evidence for a rock magnetic cause of anomalously shallow paleomagnetic inclinations from central Asia, *J. Geophys. Res.*, *108*(B2), 2107, doi:10.1029/2001JB001608.
Tarling, D. H., and P. Turner (1999), *Palaeomagnetism and Diagnesis in Sediments*, *Geol. Soc. London, Spec. Publ.*, *151*, 301 pp.
Tauxe, L., and D. Kent (1984), Properties of a detrital remanence carried by haematite from study of modern river deposits and laboratory redeposition experiments, *Geophys. J. R. Astron. Soc.*, *77*, 543–561.
Tucker, P. (1980), A particle mobility model of post-depositional realignment, *Geophys. J. R. Astron. Soc.*, *63*, 149–163.
Turcotte, D. L., and G. Schubert (1982), *Geodynamics*, 449 pp., John Wiley, Hoboken, N. J.
Tullis, T. E. (1976), Experiments on origin of slaty cleavage and schistosity, *Geol. Soc. Am. Bull.*, *87*, 745–753.
Urrutia-Fucugauchi, J., L. M. Alva-Valdivia, A. Goguitchaichvili, M. L. Rivas, and J. Morales (2004), Palaeomagnetic, rock-magnetic and microscopy studies of historic lava flows from the Paricutin volcano, Mexico: Implications for the deflection of palaeomagnetic directions, *Geophys. J. Int.*, *56*, 431–442.
Vaughn, J., K. P. Kodama, and D. P. Smith (2005), Correction of inclination shallowing and its tectonic implications: The Cretaceous Perforada Formation, Baja California, *Earth Planet. Sci. Lett.*, *232*, 71–82.
Verosub, K. L., R. A. Ensley, and J. S. Ulrick (1979), The role of water content in the magnetization of sediments, *Geophys. Res. Lett.*, *6*, 226–228.
Willis, D. G. (1977), A kinematic model of preferred orientation, *Bull. Geol. Soc. Am.*, *88*, 883–894.

S. A. Gilder, Ludwig Maximilians University, Department of Earth and Environmental Sciences, Geophysics Section, Theresienstrasse 41, D-80333 Munich, Germany. (gilder@geophysik.uni-muenchen.de)

J. Jezek, Department of Applied Mathematics and Computer Science, Faculty of Science, Charles University, Albertov 6, 128 43, Praha 2, Czech Republic. (jezek@natur.cuni.cz)